Universitat Autònoma de Barcelona

Self-Assembled Monolayers of Electroactive Molecules for the Preparation of Memory Devices

Elena Marchante Rodríguez

Thesis submitted for the award of Ph.D.

PhD Programme in Materials Science

SUPERVISORS

Dr. Marta Mas Torrent and Dr. Núria Crivillers

TUTOR

Dr. Iluminada Gallardo García

Chemistry Department / Science Faculty

Universidad Autònoma de Barcelona 2017

Molecular Switches Hot Paper

International Edition: DOI: 10.1002/anie.201508449
German Edition: DOI: 10.1002/ange.201508449

An Electrically Driven and Readable Molecular Monolayer Switch Based on a Solid Electrolyte

*Elena Marchante, Núria Crivillers, Moritz Buhl, Jaume Veciana, and Marta Mas-Torrent**

Abstract: *The potential application of molecular switches as active elements in information storage has been demonstrated through numerous works. Importantly, such switching capabilities have also been reported for self-assembled monolayers (SAMs). SAMs of electroactive molecules have recently been exploited as electrochemical switches. Typically, the state of these switches could be read out through their optical and/or magnetic response. These output reading processes are difficult to integrate into devices, and furthermore, there is a need to use liquid environments for switching the redox-active molecular systems. In this work, both of these challenges were overcome by using an ionic gel as the electrolyte medium, which led to an unprecedented solid-state device based on a single molecular layer. Moreover, electrochemical impedance has been successfully exploited as the output of the system.*

Bistable molecules that can be externally switched between two or more states with different properties have been known for a long time, and their potential as active elements in information storage devices has been recognized.[1] To move towards device miniaturization, single molecules or monolayers of molecules have been employed as active components in switches. In such systems, the input and output signals can be of different nature, such as chemical, optical, magnetic, or electrical. However, electrical signals are particularly appealing as they can be more easily integrated with current technologies. Single electroactive molecules have been incorporated in three terminal junctions, where an electrical field generated by applying a voltage to a gate terminal was employed to modulate the molecular charge, and the current that passed through the molecule connecting two contacts was used as the readout mechanism.[2] Although scientifically extremely motivating, these devices are technologically very demanding and currently show poor fabrication yields and device reproducibility. The preparation of hybrid surfaces that consist of inorganic conducting supports functionalized with a chemically bonded self-assembled monolayer (SAM) offers a clear alternative platform for the preparation of molecular devices.[3]

The preparation of SAMs from solution by spontaneous surface self-organization of the molecules is an inexpensive as well as powerful and versatile method for the modification of surfaces at the molecular level. SAMs of electroactive molecules have been exploited as electrochemical switches in the last few years.[4] Typically, the state of these switches could be read out through their optical and/or magnetic response.[5] Despite the extremely encouraging results achieved thus far, two main bottlenecks have been clearly identified, which seriously hamper the progress in the field towards real applications: 1) The reading processes that are required to determine the output signals are difficult to integrate into devices, and 2) to switch between the different accessible redox states of the molecular systems, solutions containing an electrolyte are required to stabilize the charged states (i.e., ion pairing) and to ensure ionic conductivity in the electrochemical cell. Herein, we overcome both of these challenges by employing SAMs with an electroactive ferrocene (Fc) unit in a dual approach. First, electrochemical impedance spectroscopy (EIS) was used to measure the capacitance of the SAM to be employed as the output signal of the switch. Second, a solid-state device based on such a single molecular layer as the active component was prepared using a solid electrolyte medium. These results represent a step forward in the field, improving the perspectives of employing hybrid surfaces as molecular switches for their future integration in electronic applications.

SAMs of ferrocenyl alkylthiol derivatives on gold have been established as reference systems in electrochemical studies of surface-confined molecules.[6] For this reason, SAMs of 11-(ferrocenyl)undecanethiol ($FcC_{11}SH$) were employed as switchable redox units as ferrocene exhibits two accessible redox states (i.e., the neutral and oxidized redox states; Figure 1a). The electrochemical cell shown in Figure 1b was thus fabricated. Three coplanar gold electrodes (counter (CE), working (WE), and reference electrode (RE)) were thermally evaporated through a mask on a glass substrate, and a silicon mold or a Teflon ring were used to delimit a fixed area of the electrolyte in contact with the electrodes. The Au WE was modified with the ferrocene SAM by immersion in a 1 mM solution of $FcC_{11}SH$ in ethanol for 18 hours (Figure S1).

The electrochemical properties of the SAMs were first investigated using an ionic liquid (IL) as the electrolyte. Figure 1c shows the cyclic voltammogram (CV) of the Fc-SAM obtained when using 1-ethyl-3-methylimidazoliumbis-(trifluoromethylsulfonyl) imide (EMIM-TFSI) as the electrolyte and employing the electrochemical cell described above. A redox peak was observed at $E^{1/2} = 0.23$ V (vs. Au at a scan rate of 200 mV s^{-1}), which corresponds to the Fc/Fc$^+$ pair. The almost insignificant voltage difference observed between the cathodic and anodic peak ($\Delta E = 22$ mV at 200 mV s^{-1}) is

[*] E. Marchante, Dr. N. Crivillers, M. Buhl, Prof. J. Veciana, Dr. M. Mas-Torrent
Institut de Ciència de Materials de Barcelona (ICMAB-CSIC) and CIBER-BBN
Campus de la UAB, 08193 Bellaterra (Spain)
E-mail: mmas@icmab.es

Supporting information for this article is available on the WWW under http://dx.doi.org/10.1002/anie.201508449.

 © 2016 Wiley-VCH Verlag GmbH & Co. KGaA, Weinheim

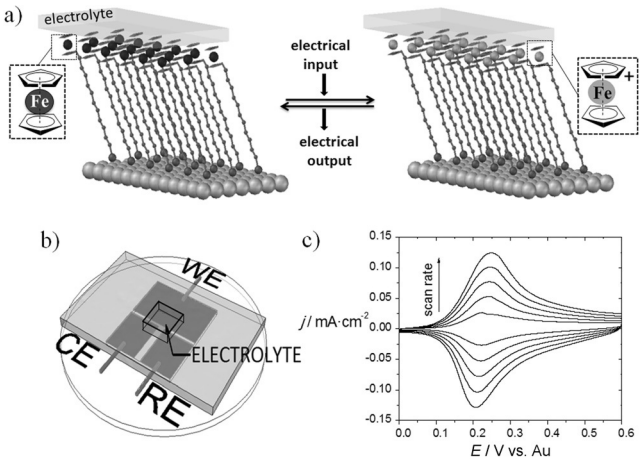

Figure 1. a) Molecular switch based on a ferrocene SAM on gold. b) Home-made electrochemical cell with three coplanar gold electrodes. c) Cyclic voltammograms of the Fc-SAM at different scan rates (100, 200, 300, 400, and 500 $mV\,s^{-1}$) using a modified gold working electrode and gold reference and counter electrodes and the ionic liquid EMIM-TFSI.

characteristic of surface-confined molecules, which was further confirmed by the linear dependence of the current density of the redox peak (J_p) on the scan rate in the range of 50–500 $mV\,s^{-1}$ (Figure S2).[7] A surface coverage of 3.7×10^{-10} $mol\,cm^{-2}$ was estimated, which is slightly lower than the reported theoretical value (4.5×10^{-10}).[8] The observed smaller number of electroactive sites within the SAM could be explained by the large size of the $TFSI^-$ anion, which controls the ion pairing. As reported, if the anion cannot fully compensate the positive charges of all Fc^+ ions, some of the Fc units will appear to be non-electroactive.[9]

Electrochemical impedance spectroscopy (EIS) is a powerful method to characterize the electrical properties of interfaces.[10–12] Here, EIS was exploited to measure the capacitance of the different redox states of the switchable SAM. In an ideal situation, the gold metal surface would act as one of the capacitor plates, and the physisorbed ions at the SAM/electrolyte interface would act as the other capacitor plate.[13]

EIS measurements were performed at two different applied DC biases, before ($V_0=+10$ mV) and after ($V_1=+450$ mV) the redox peak, which define the states 0 and 1 of the switch (see the Supporting Information for experimental details). The Bode magnitude plot (impedance modulus ($|Z|$) vs. frequency) is shown in Figure 2a. At low frequencies, the graphs for the two states are two parallel straight lines with slopes of approximately −0.9. This behavior is characteristic of capacitor-like systems, and the deviation from a slope of −1 can be explained by capacitance dispersion owing to the adsorption of ions on the electrodes and the roughness of the electrode surface.[14] Accordingly, in the Bode phase plot (φ vs. f), the phase angle slightly deviates from 90° at low frequency, which would be expected for an ideal ionic insulator (Supporting Information, Figure S3a).[12a] Remarkably, a significant decrease in $|Z|$ of one order of magnitude was observed between state 0 and state 1 at low frequencies, indicating that the impedance can be used as a readout of the molecular switch. For comparison, the same experiments were performed with undecanethiol SAMs, but no impedance differences were observed when different DC biases were applied to the functionalized WE in this frequency region (Figure S4). This result indicates that the changes observed in $|Z|$ for the Fc-SAMs do not arise from the simple polarization of the electrode/electrolyte interface by the applied voltage; instead, the redox state of the electroactive species plays a crucial role.

At higher frequencies ($f>10$ kHz), the frequency-independent impedance (Figure 2a) and a phase angle close to zero (Figure S3a,c) indicate that the system behaves as a resistor, that is, the total impedance is dominated by the solution resistance.[13] This is due to the fact that at high frequencies, the capacitor behaves as a short-circuit element as the charging time is too short, allowing the AC current to pass.

The EIS results can also be presented in the form of the real or imaginary part of the interfacial complex capacitance as a function of frequency. The real part of the capacitance per unit area (C_{re}) was calculated by the following equation:[15]

$$C_{re}(f)=\frac{1}{2\pi f}\frac{Z_{im}}{\left[Z_{re}^2+Z_{im}^2\right]}\frac{1}{A} \quad (1)$$

where A is the area of the working electrode, Z_{re} and Z_{im} are the real and imaginary parts of the complex impedance, respectively, and f is the frequency.

The dependence of the C_{re} value on the frequency for the Fc-SAMs at both applied DC bias voltages is shown in Figure 2b. At high frequencies, the measured capacitance corresponds to the bulk capacitance, whereas at low frequencies, a plateau was reached, reflecting the interfacial capacitance.[15c] The C_{re} value measured at 1 Hz is significantly different for state 0 ($V=10$ mV) and state 1 ($V=450$ mV). Such large on/off ratios in the capacitance measured for the two states ($\Delta C_{re}=44$ $\mu F\,cm^{-2}$) make it possible to use this parameter to follow the switching. We attribute this difference in capacitance mainly to the charges accumulated at the

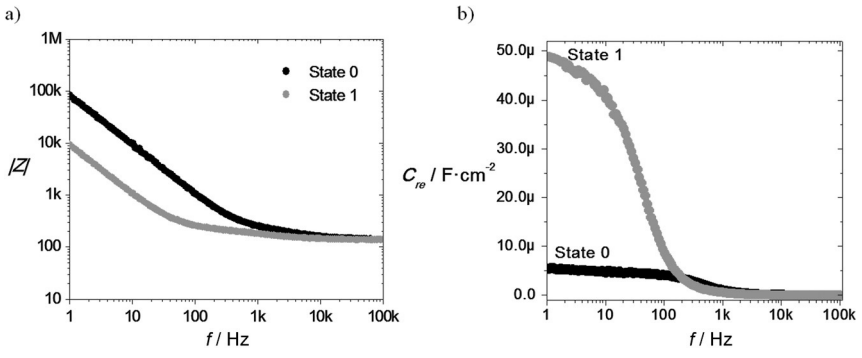

Figure 2. a) Bode magnitude plot ($|Z|$ vs. f). b) The real part of the complex capacitance as a function of frequency (C_{re} vs. f) for Fc-SAM on Au using EMIM-TFSI as the electrolyte. Black line: state 0 at +10 mV, gray line: state 1 at +450 mV.

 © 2016 Wiley-VCH Verlag GmbH & Co. KGaA, Weinheim

electrode interface, which are influenced by the redox state of the Fc molecules, although a certain contribution from structural changes in the SAM cannot be ruled out completely.[16] Overall, it was demonstrated that the investigated surface-confined electrochemical switch can be electrically driven as well as read.

A second important challenge in the field is the lack of solid-state devices with such electrochemically switchable SAMs. To overcome this issue, an ionic gel (IG) was employed as the electrolyte medium. Generally, IGs are prepared by entrapping an IL in a polymer matrix.[17] IGs have already been exploited in several electronic devices, such as in inorganic electrochemical transistors,[18] as photoactuated microvalves,[19] and as high-capacitance gate dielectrics.[20] However, to the best of our knowledge, this is the first time that a solid electrolyte has been employed to electrochemically control a molecular redox switch grafted onto a surface.

The IG based on poly(vinylidene fluoride-*co*-hexafluoropropylene) (PVDF-HFP) and EMIM-TFSI (1:4) was prepared as described in the literature (Figure S5 and S7).[20a,b] The IG acetone solution was drop-casted onto the modified gold electrodes, with the active area limited by the silicon mold, in a chamber with an inert and low-humidity atmosphere. After solvent evaporation and solidification of the gel mixture, the sample was removed from the glove box and analyzed in air. Figure 3a shows a photograph of the solid-state device based on the IG film.

As shown in Figure 3b, the CV electrochemical characteristics of the Fc-SAM could be successfully determined by using co-planar electrodes coated with the transparent, flexible, and solid IG. Remarkably, the CV could also be measured by employing a thin film of an IG that was prepared first on a glass slide and then transferred with tweezers and laminated on top of the three gold coplanar electrodes, with the WE modified with the ferrocene SAM. The cyclic voltammogram thus obtained showed very similar features as the ones shown in Figure 3b (see also Figure S7).

When the CV obtained with the solid electrolyte is compared to the one obtained with the IL, there are few differences in the electrochemical characteristics commonly used for evaluating the response of surface-grafted molecules. In the case of the IG, a larger peak-to-peak voltage difference (ΔE) was observed, which also depended more strongly on the scan rate. This is indicative of a slower electron-transfer process, which is expected to occur because of the lower ion mobility in the solid IG film. Furthermore, a lower current density was observed for the IG despite the fact that the density of the ferrocene molecules grafted onto the gold electrode should be very similar to that of the SAMs studied with the IL. In other words, the number of redox-active ferrocene species electrochemically visualized is considerably lower when the IG is used. This can be explained in terms of the less homogeneous and intimate contact between the IG and the SAM as well as the less effective charge compensation of the ferrocinium molecules with the $TFSI^-$ ion, which is again probably due to the more limited ion diffusion at the solid-state interface. This observation can be quantified by the integration of the CV redox peaks; it was found that the number of molecules that participate in the electrochemical process is reduced to 30–50% on going from the IL to the IG device.

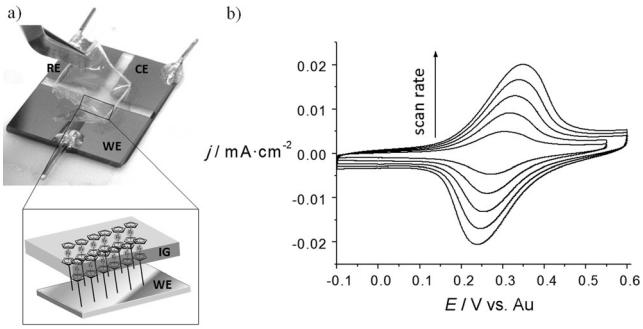

Figure 3. a) The three coplanar gold working (WE), counter (CE), and reference (RE) electrodes with the IG electrolyte (top). Scheme of the area between the WE modified with Fc-SAM and the solid electrolyte (bottom). b) Cyclic voltammograms of the Au/Fc-SAM/solid IG device at different scan rates (100, 200, 300, 400, and 500 $mV s^{-1}$).

Interestingly, EIS measurements were also used to follow the switching process in this solid-state device. In this case, state 0 and state 1 were written using a DC voltage of 10 mV and 600 mV vs. Au, respectively (see the corresponding cyclic voltammogram in Figure S8). The dependence of the impedance modulus, $|Z|$, on the frequency of the solid-state device is depicted in Figure 4a. As before, there is a clear diminution of the impedance value on going from state 0 to state 1, although this time, the variation is smaller. Furthermore, a noticeable difference is that in the case of the IL-based device, the on/off ratio of the $|Z|$ values between the two states is maintained constant in the range 1–100 Hz, whereas in the IG device, the plots corresponding to the two states start to converge in the region of 10–100 Hz. This could again be caused by the lower mobility of the ions in the gel

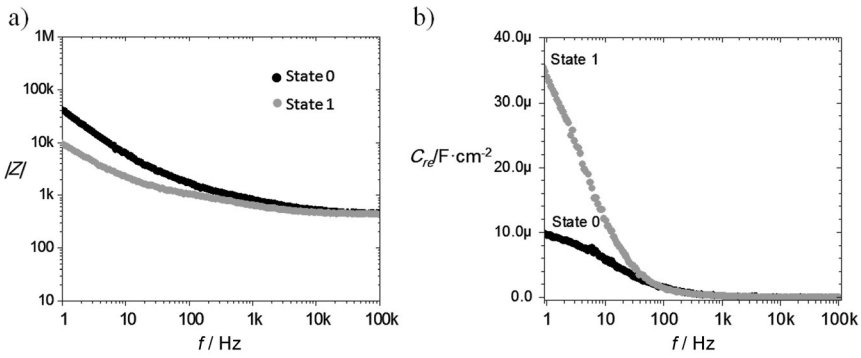

Figure 4. a) Bode magnitude plot ($(|Z|)$ vs. f). b) Real part of the capacitance as a function of frequency for the electrochemical device, with the solid IG as the electrolyte. State 0 (black) and state 1 (gray) correspond to DC applied biases of 10 mV and 600 mV, respectively.

 © 2016 Wiley-VCH Verlag GmbH & Co. KGaA, Weinheim

preventing the formation of a compensated double layer at lower frequencies.

The C_{re} value was calculated as explained above for the IL-based switch (Figure 4b). The C_{re} values at 1 Hz in state 0 for the IL and IG devices are very similar, namely 5.3 $\mu F\,cm^{-2}$ and 9.25 $\mu F\,cm^{-2}$, respectively. Although the on/off ratio is lower for the IG-based device than for the IL device, the ΔC_{re} value is still outstanding, 25 $\mu F\,cm^{-2}$ at 1 Hz.

To explore the stability of the switch, it was subjected to 100 switching cycles, and the C_{re} values measured at 1 Hz were plotted as a function of the cycle number for both electrolyte media, namely IL (Figure 5a) and IG (Figure 5b).

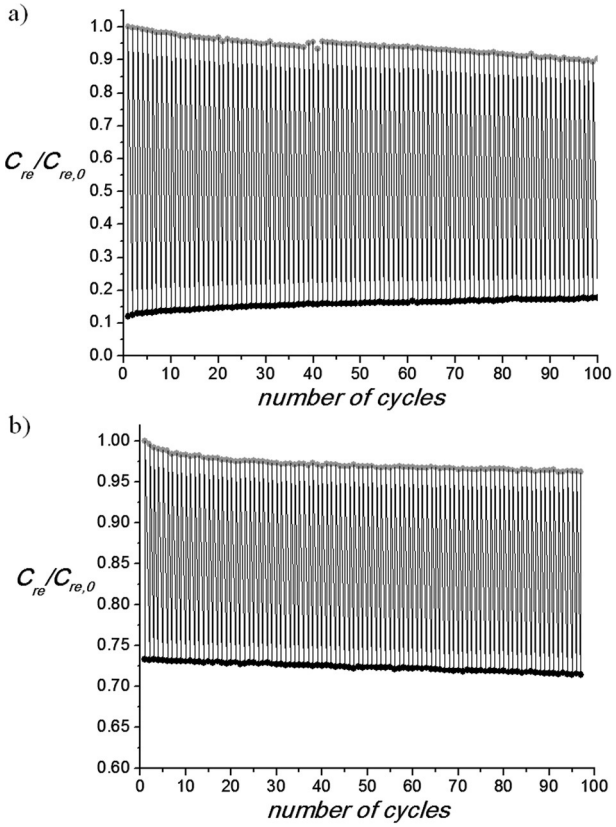

Figure 5. $C_{re}/C_{re,0}$ (at 1 Hz) switching over 100 cycles by alternating the applied bias with a) the IL and b) the IG as the electrolyte for state 0 (black) and state 1 (gray).

There was a small decrease in the on/off ratio under the IL conditions, which we attribute to ion permeation, which can additionally cause some molecular desorption. Remarkably, despite the lower on/off ratio, the stability of the switchable system, that is, the switching fatigue, was improved by the use of the solid electrolyte. This finding demonstrates the feasibility of using the C_{re} value as the output of the switch even when using a solid-state electrochemical device.

In summary, we have demonstrated that it is possible to write and read an electrochemical switch that is based on a self-assembled monolayer of an electroactive molecule by using an electrical input to control the switch as well as an electrical output to monitor it. This has been achieved not only in liquid environments but also in a solid-state device based on an ion gel electrolyte. The method employed here is inexpensive and simple and could also be extended to other redox-active molecules. These results represent a proof-of-concept study of a feasible approach for the integration of molecular-monolayer-based electrochemical switches.

Acknowledgements

We thank R. Pfattner for his help and F. J. del Campo for providing the silicon mold. We acknowledge financial support from the EU (projects ERC StG 2012-306826 e-GAMES, ITN iSwitch 642196, and CIG PCIG10-GA-2011-303989), the Networking Research Center of Bioengineering, Biomaterials and Nanomedicine (CIBER-BBN), the DGI (Spain; BE-WELL CTQ2013-40480-R), and the Generalitat de Catalunya (2014-SGR-17). E.M. and N.C. acknowledge the Materials Science PhD program of the UAB and the JdC program, respectively.

Keywords: electrochemical impedance spectroscopy · ferrocene · molecular switches · self-assembled monolayers · solid electrolytes

How to cite: *Angew. Chem. Int. Ed.* **2016**, *55*, 368–372
Angew. Chem. **2016**, *128*, 376–380

[1] a) J. Andréasson, U. Pischel, *Chem. Soc. Rev.* **2010**, *39*, 174–188; b) J. E. Green, J. W. Choi, A. Boukai, Y. Bunimovich, E. Johnston-Halperin, E. DeIonno, Y. Luo, B. A. Sheriff, K. Xu, Y. S. Shin, H.-R. Tseng, J. F. Stoddart, J. Heath, *Nature* **2007**, *445*, 414–417; c) V. Ferri, M. Elbing, G. Pace, M. D. Dickey, M. Zharnikov, P. Samorì, M. Mayor, M. A. Rampi, *Angew. Chem. Int. Ed.* **2008**, *47*, 3407–3409; *Angew. Chem.* **2008**, *120*, 3455–3457.

[2] a) C. Huang, A. V. Rudnev, W. Hong, T. Wandlowski, *Chem. Soc. Rev.* **2015**, *44*, 889–901; b) M. L. Perrin, E. Burzurí, H. S. J. van der Zant, *Chem. Soc. Rev.* **2015**, *44*, 902–919; c) N. Darwish, A. C. Aragonès, T. Darwish, S. Ciampi, I. Díez Pérez, *Nano Lett.* **2014**, *14*, 7064–7070.

[3] a) V. Balzani, A. Credi, M. Venturi, *ChemPhysChem* **2008**, *9*, 202–220; b) M. Mas-Torrent, C. Rovira, J. Veciana, *Adv. Mater.* **2013**, *25*, 462–468; c) B. K. Pathem, S. Claridge, Y. B. Zheng, P. S. Weiss, *Annu. Rev. Phys. Chem.* **2013**, *64*, 605–630.

[4] a) Z. Liu, A. A. Yasseri, J. S. Lindsey, D. F. Bocian, *Science* **2003**, *302*, 1543–1545; b) G. Periyasamy, R. D. Levine, F. Remacle, *Aust. J. Chem.* **2010**, *63*, 173–183.

[5] a) G. de Ruiter, M. E. van der Boom, *Angew. Chem. Int. Ed.* **2012**, *51*, 8598–8601; *Angew. Chem.* **2012**, *124*, 8726–8729; b) A. D. Shukla, A. Das, M. E. van der Boom, *Angew. Chem. Int. Ed.* **2005**, *44*, 3237–3240; *Angew. Chem.* **2005**, *117*, 3301–3304; c) C. Simão, M. Mas-Torrent, J. Casado-Montenegro, F. Otón, J. Veciana, C. Rovira, *J. Am. Chem. Soc.* **2011**, *133*, 13256–13259; d) C. Simão, M. Mas-Torrent, N. Crivillers, V. Lloveras, J. M. Artés, P. Gorostiza, J. Veciana, C. Rovira, *Nat. Chem.* **2011**, *3*, 359–364.

[6] A. V. Rudnev, U. Zhumaev, T. Utsunomiya, C. Fan, Y. Yokota, K.-i. Fukui, T. Wandlowski, *Electrochim. Acta* **2013**, *107*, 33–44.

[7] H. Ju, D. Leech, *Phys. Chem. Chem. Phys.* **1999**, *1*, 1549–1554.

[8] C. A. Nijhuis, W. F. Reus, G. M. Whitesides, *J. Am. Chem. Soc.* **2009**, *131*, 17814–17827.

[9] Q.-W. Sun, K. Murase, T. Ichii, H. Sugimura, *J. Electroanal. Chem.* **2010**, *643*, 58–66.

 © 2016 Wiley-VCH Verlag GmbH & Co. KGaA, Weinheim

[10] *Impedance Spectroscopy: Theory, Experiment, and Applications*, 2nd ed. (Eds.: E. Barsoukov, J. R. Macdonald), Wiley, Hoboken, **2005**.
[11] a) R. E. Ruther, Q. Cui, R. J. Hamers, *J. Am. Chem. Soc.* **2013**, *135*, 5751 – 5761; b) P. Brooksby, K. Anderson, A. Downard, A. Abell, *J. Phys. Chem. C* **2011**, *115*, 7516 – 7526; c) B. P. G. Silva, D. Z. de Florio, S. Brochsztain, *J. Phys. Chem. C* **2014**, *118*, 4103 – 4112.
[12] a) E. Boubour, R. B. Lennox, *J. Phys. Chem. B* **2000**, *104*, 9004 – 9010; b) W. Wang, S. Zhang, P. Chinwangso, R. C. Advincula, T. R. Lee, *J. Phys. Chem. C* **2009**, *113*, 3717 – 3725; c) D. K. Peng, S. T. Yu, D. J. Alberts, J. Lahann, *Langmuir* **2007**, *23*, 297 – 304; d) C. A. Nijhuis, B. A. Boukamp, B. J. Ravoo, J. Huskens, D. N. Reinhoudt, *J. Phys. Chem. C* **2007**, *111*, 9799 – 9810.
[13] E. Boubour, R. B. Lennox, *Langmuir* **2000**, *16*, 4222 – 4228.
[14] a) T. Pajkossy, *Electroanal. Chem.* **1994**, *364*, 111 – 125; b) Z. Kerner, T. Pajkossy, *Electrochim. Acta* **2000**, *46*, 207 – 211; c) T. Pajkossy, *Solid State Ionics* **2005**, *176*, 1997 – 2003.
[15] a) E. Katz, O. Lioubashevsky, I. Willner, *J. Am. Chem. Soc.* **2004**, *126*, 15520 – 15532; b) T. M. Nahir, E. F. Bowden, *Langmuir* **2002**, *18*, 5283 – 5296; c) C. R. Mariappan, T. P. Heins, B. Roling, *Solid State Ionics* **2010**, *181*, 859 – 863.
[16] N. Darwish, P. K. Eggers, S. Ciampi, Y. Zhang, Y. Tong, S. Ye, M. N. Paddon Row, J. J. Gooding, *Electrochem. Commun.* **2011**, *13*, 387 – 390.
[17] a) M. J. Park, I. Choi, J. Hong, O. Kim, *J. Appl. Polym. Sci.* **2013**, *129*, 2363 – 2376.
[18] D. Khodagholy, V. F. Curto, K. J. Fraser, M. Gurfinkel, R. Byrne, D. Diamond, G. G. Malliaras, F. Benito-Lopez, R. M. Owens, *J. Mater. Chem.* **2012**, *22*, 4440 – 4443.
[19] F. Benito-Lopez, R. Byrne, R. A. M., N. E. Vrana, G. McGuinness, D. Diamond, *Lab Chip* **2010**, *10*, 195 – 201.
[20] a) K. H. Lee, M. S. Kang, S. Zhang, Y. Gu, T. P. Lodge, C. D. Frisbie, *Adv. Mater.* **2012**, *24*, 4457 – 4462; b) K. H. Lee, S. Zhang, T. P. Lodge, C. D. Frisbie, *J. Phys. Chem. B* **2011**, *115*, 3315 – 3321; c) B. J. Kim, H. Jang, S.-K. Lee, B. H. Hong, J.-H. Ahn, J. H. Cho, *Nano Lett.* **2010**, *10*, 3464 – 3466.

Received: September 14, 2015
Published online: October 28, 2015

 © 2016 Wiley-VCH Verlag GmbH & Co. KGaA, Weinheim

Angewandte Chemie
Eine Zeitschrift der Gesellschaft Deutscher Chemiker

Supporting Information

An Electrically Driven and Readable Molecular Monolayer Switch Based on a Solid Electrolyte

*Elena Marchante, Núria Crivillers, Moritz Buhl, Jaume Veciana, and Marta Mas-Torrent**

anie_201508449_sm_miscellaneous_information.pdf

Supporting Information

Table of contents

page

Experimental methodologies

Materials and reagents. HPLC solvents, dichloromethane, acetone, absolute ethanol and acetonitrile were supplied by Teknokroma from Ionic liquids, 1-Ethyl-3-methylimidazolium bis(trifluoromethylsulfonyl)imide (EMIM-TFSI, **IL1**), 1-Ethyl-3-methylimidazolium tetrafluoroborate (EMIM-BF_4, **IL2**), 1-Ethyl-3-methylimidazolium ethyl sulphate (EMIM-$EtSO_4$, (**IL3**) were supplied by Aldrich and dried under vacuum at 70 ºC for 24h prior to their use. Tetrabutylammonium hexafluorophosphate (Bu_4NPF_6), 11-(ferrocenyl)undecanethiol ($Fc(CH_2)_{11}SH$) were supplied by Aldrich and used as received.

EMIM-TFSI, **IL1** EMIM-BF_4, **IL2** EMIM-$EtSO_4$, **IL3**

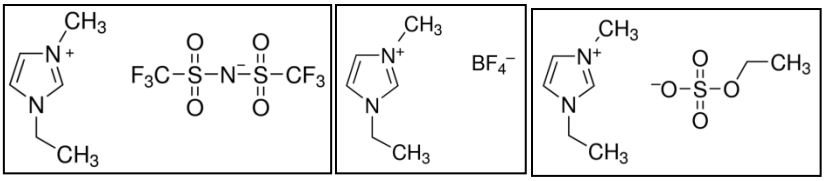

Poly(vinylidene fluoride-co-hexafluoropropylene) average Mw ~400,000, average Mn ~130,000, pellets (**PVDF-HFP)** was purchased from Sigma-Aldrich.

PVDF-HFP

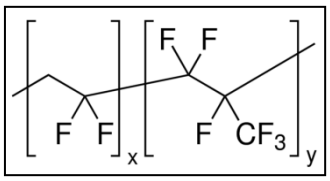

Gold electrode preparation. Gold electrodes were prepared through a home-made mask by evaporating 15 nm of chromium layer, as adhesion layer, and 75 nm gold on a glass slide of 1 mm of thickness. A System Auto 306 from Boc Edwards evaporator was used for the thermal evaporation of Au and Cr.

Experimental Prodecures

Self-assembled monolayers preparation: First, the gold electrodes were rinsed with different solvents, increasing polarity, dichloromethane, acetone and ethanol, and dried under a nitrogen stream. Then, substrates were exposed to ozone in a UV ozone chamber for 20 minutes and the cleaned for at least 30 minutes in ethanol. Finally the substrates were rinsed with isopropanol and dried under a N_2 stream before immersing them in the ferrocene solution. The ferrocene SAMs on the working electrode (WE) were prepared under light exclusion and under inert atmosphere. The substrates were immersed in a 1 mM solution of 11-(ferrocenyl)undecanethiol ($Fc(CH_2)_{11}SH$) in ethanol at ambient conditions (25 ± 3°C) for 18 h. To avoid the surface functionalization of the counter and reference gold electrodes, the substrate was placed vertically using a teflon holder, and only the WE was immersed into the $Fc(CH_2)_{11}SH$ solution. The samples were then removed from the solution and rinsed with large amounts of ethanol to remove physisorbed material and finally dried with N_2. All solvents used in monolayer preparation were of HPLC grade. SAMs of undecanethiol were prepared following the same methodology.

Preparation of the ion-gel: For the preparation of the ion-gel, initially, the polymer (PVDF-HFP) is dissolved in acetone in a weight ratio 1:10 of polymer to solvent. The polymer solution is stirred continuously until a homogeneous mixture is achieved. Then the ionic liquid (EMIM-TFSI) is added to the solution in a ratio 1:4 of polymer to IL. The solution was prepared at room temperature and argon atmosphere. The drop-casting method is used for the preparation of the ion-gels onto the planar home-made electrochemical cell delimiting the area with a silicon mask. The films were prepared inside an argon atmosphere glovebox ($[O_2]$ < 1 ppm; $[H_2O]$ < 1.5 ppm), where the solvent was allowed to evaporate slowly.

Electrochemical Impedance Spectroscopy (EIS) measurements: The EIS experiments were recorded by using a Bio-Logic VMP3 potentiostat and employing the homemade

electrochemical cell. The impedance measurements were obtained at two different dc potentials that does not overlap with the Faradaic process (before and after the redox process in each case), and were superimposed on a sinusoidal potential modulation of ±5 mV (Vrms). The resulting current was recorded over a frequency domain of 100 KHz to 1 Hz. Thirty points, equally spaced on a logarithmic scale, were acquired per decade increment in frequency. All experiments were performed at room temperature and under environmental conditions.

Switching Measurements. The AC impedance switching process was recorded at 1Hz using a Novocontrol Alpha-AN impedance analyzer equipped with a potentiostat POT/GAL 30V/2A electrochemical interface. A low AC voltage of 5 mV was superimposed at two different applied DC bias, before and after the redox peak (*state 0* and *state 1*, respectively). These cycling experiments were performed by pre-biasing the sample at the corresponding DC voltage for each state, during 5 seconds in the case of the ionic liquid and 15 seconds for the solid ion-gel.

Apparatus

Cyclic Voltammetry (CV): CV measurements were performed with a potentiostat-galvanostat VersaSTAT3 from Princeton Applied Research, in a homemade electrochemical cell.

Electrochemical Impedance Spectroscopy (EIS). The EIS frequency spectra were recorded by using a Bio-Logic VMP3 potentiostat and employing the homemade electrochemical cell. The AC impedance switching process was recorded at 1Hz of frequency using a Novocontrol Alpha-AN impedance analyzer equipped with a POT/GAL 30 V/2 A electrochemical interface.

FT-IR: Spectrum One FT-IR Spectrometer from Perkin Elmer with the universal ATR Polarization accessory.

Atomic Force Microscopy (AFM): 5100 SPM system from Agilent Technologies

Scanning electron microscope (SEM): SEM images were acquired in a QUANTA FEI 200 FEG-ESEM.

Surface coverage calculation:

From the conventional equation[1]: $\Gamma = Q/nFA$

where Γ is the surface concentrations in mol cm^{-2}, Q is the integrated area of the anodic or cathodic charge, n is the number of electrons transferred (=1), F is Faraday's constant, and A is the electrode surface area.

SUPPORTING INFORMATION FIGURES

The evaporated gold showed a roughness of 2.45 ± 0.37 nm (root mean square (RMS)) extracted from intermittent atomic force microscopy images.

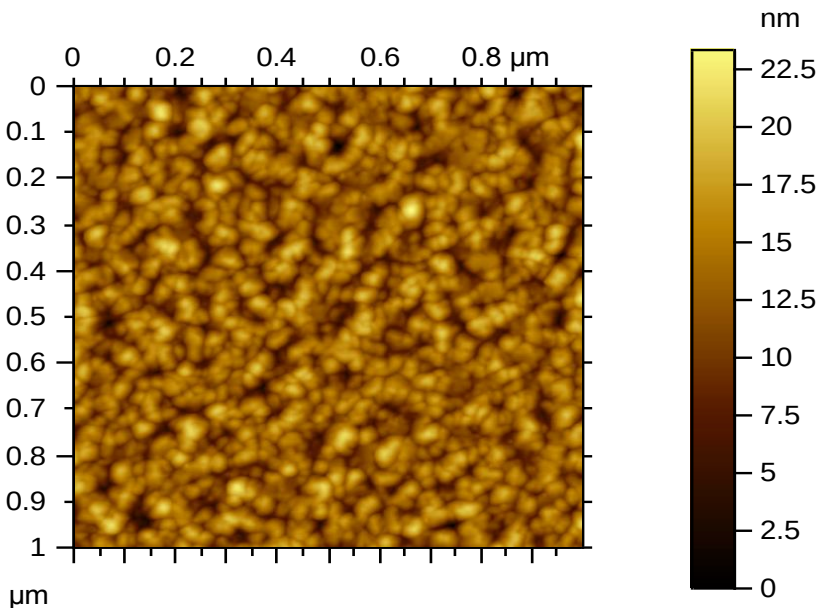

Figure S1. Intermittent Atomic Force Microscopy (AFM) image of the freshly evaporated gold used as electrodes (75 nm Au on 15nm Cr as adhesion layer).

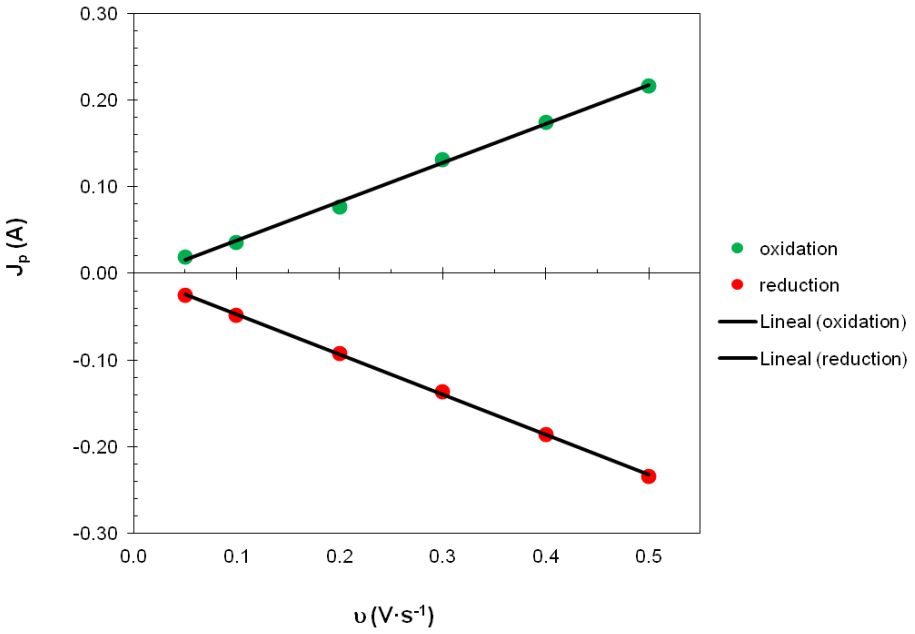

Figure S2. Dependence of current density (J_p) with the scan rate (ν).

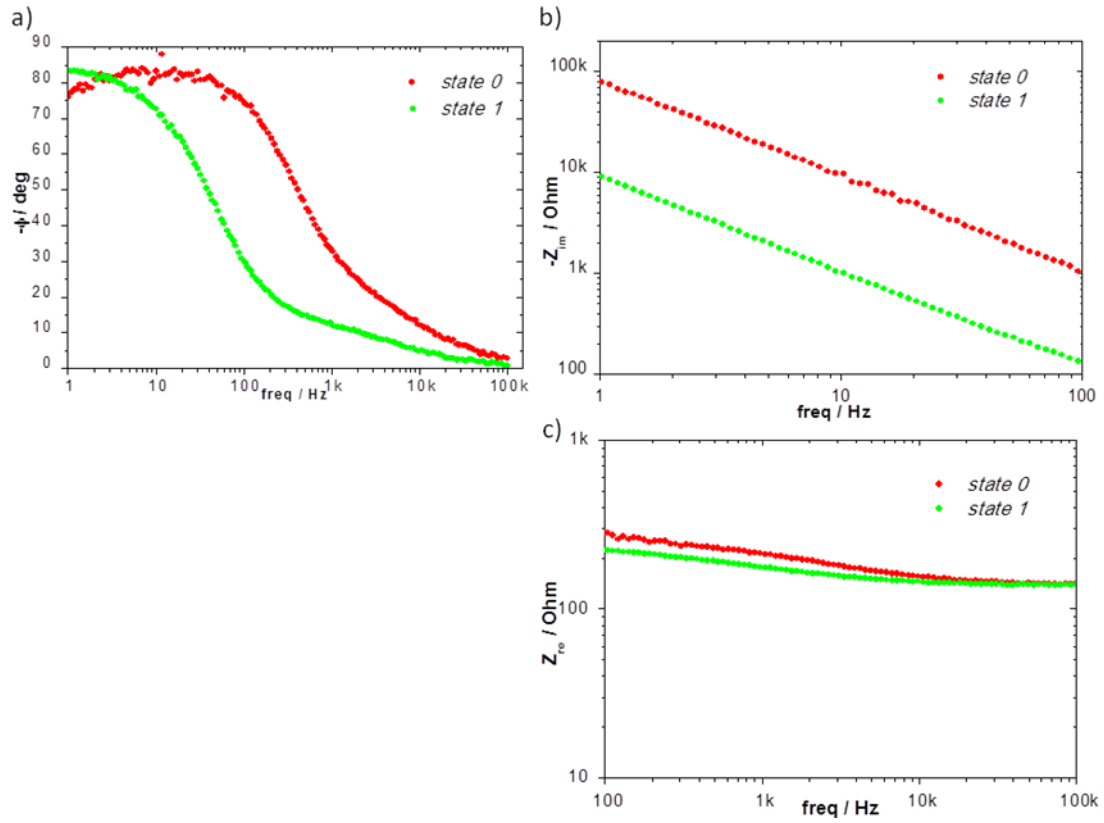

Figures S3. a) Phase angle versus frequency plot, b) $-Z_{im}$ versus frequency below 100 Hz (where the capacitive contribution is prevailing) and c) Z_{re} versus frequency above 100 Hz (where the resistive contribution is dominant), acquired for the $FcC_{11}SH$ SAM on gold using EMIM-TFSI as electrolyte. All graphs are shown for *state 0* and *state 1*.

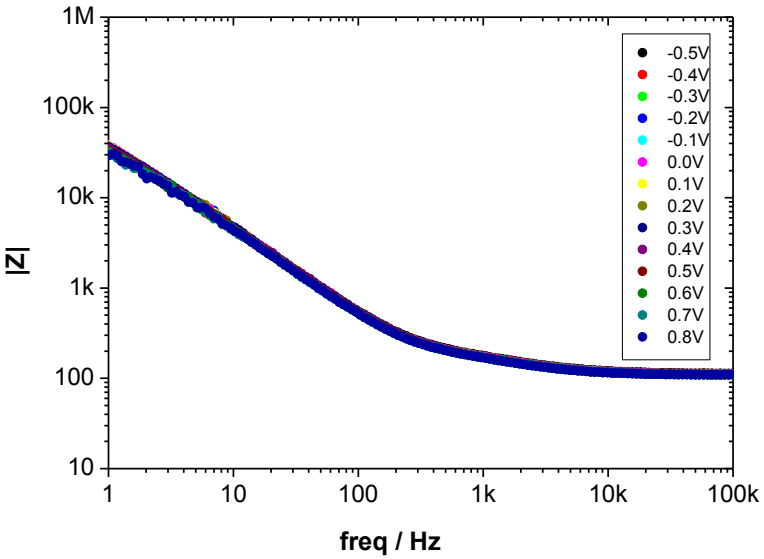

Figure S4. Module Bode plot for the alkanethiol SAM with the ionic liquid (EMIM-TFSI) as electrolyte.

Different ion-gel film thicknesses were tested by changing the volume of the drop cast ion-gel solutions. The films thicknesses were measured by Scanning Electron Microscopy (SEM). The most optimum CV response, considering the lower ΔE (difference between oxidation and reduction peaks), was achieved in films in the range of 250-300 µm thick (Figure S6). Further, the structure of the ion-gel film was characterized by IR without showing variation of the characteristic bands with time under environmental conditions (Figure S7).

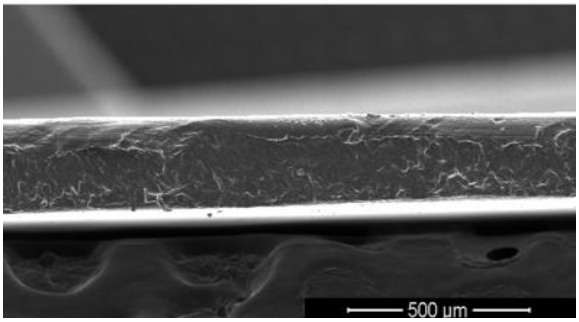

Figure S5. Scanning electron microscopy image of the profile of an ion-gel film employed for the electrochemical (CV and EIS) experiments.

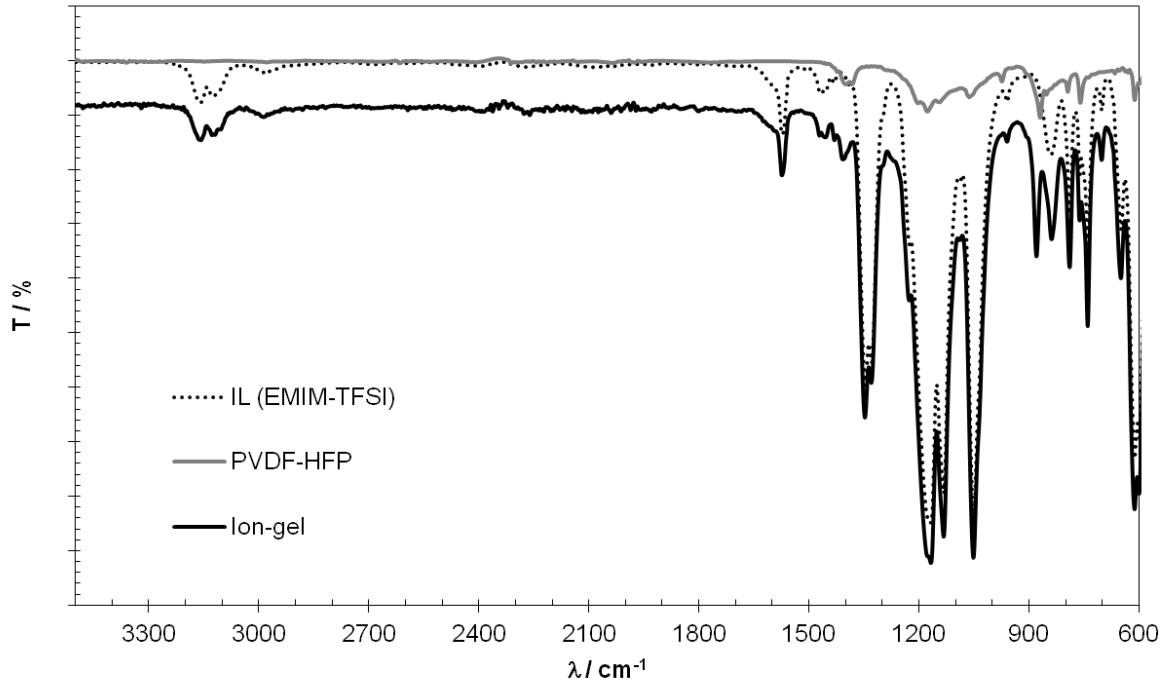

Figure S6. FT-IR spectrum of the IL1 (EMIM-TFSI), the polymer PVDF-HFP and the ion-gel. Different FT-IR spectra were taken during several days and, compared to the freshly prepared ion-gel any modification was observed.

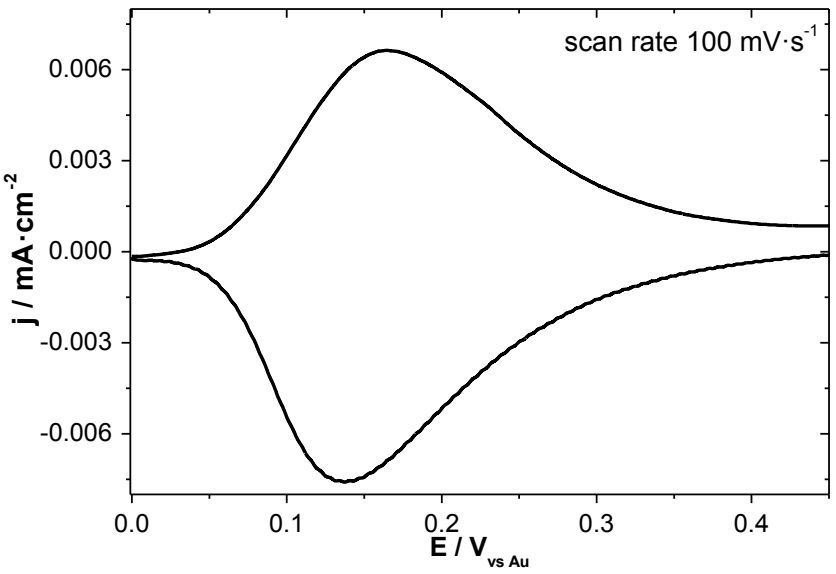

Figure S7. CV of the Fc-SAM with the IG prepared ex-situ and place it on top of the modified gold electrode. The ion-gel was prepared and transferred on top of the 3-gold flat electrodes under room conditions (25ºC and approximately a humidity level of 55%). Scan rate = 100 mV/s.

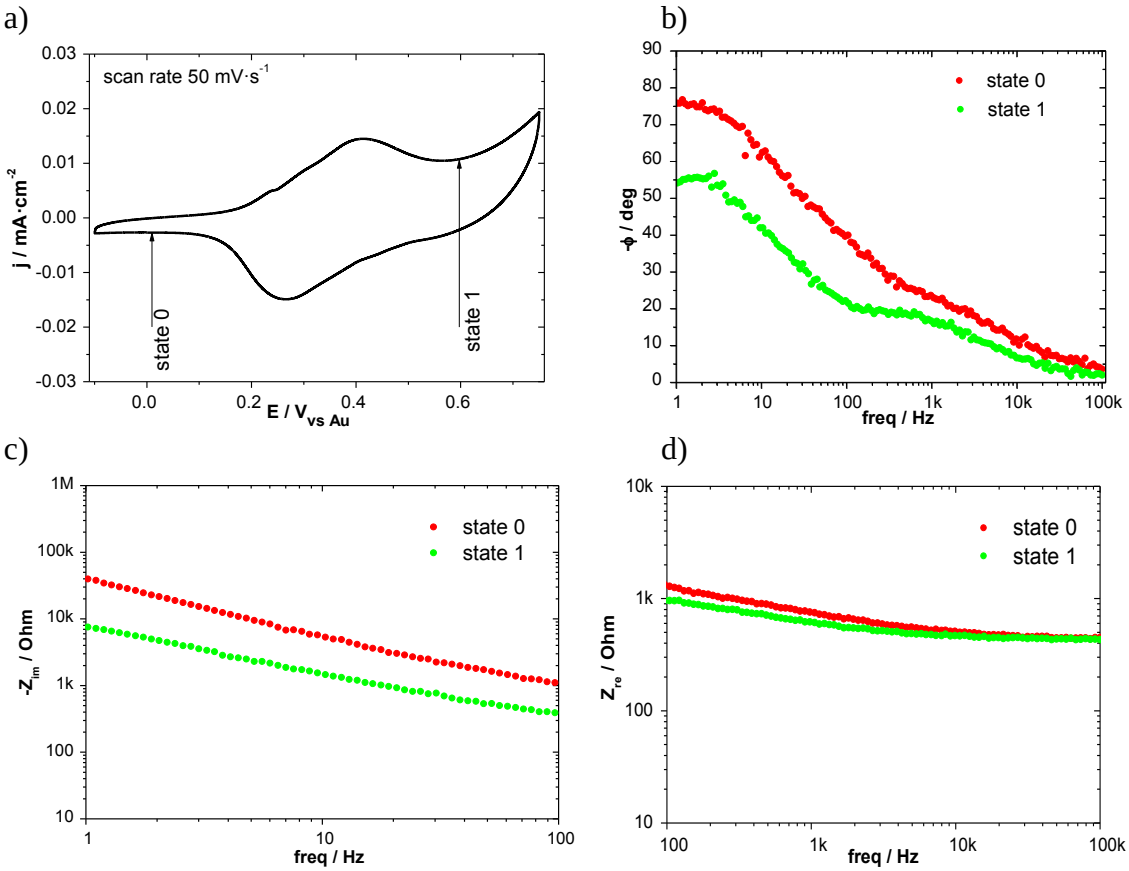

Figures S8. a) Cyclic voltammetry, at a scan rate of 50 mV/s, of the $FcC_{11}S$-Au SAM with the ion-gel prepared on top of the 3-gold flat electrodes, b) phase angle versus frequency plot for *state 0* and *state 1*, c) $-Z_{im}$ versus frequency below 100 Hz (where the capacitive contribution is dominant) and d) Z_{re} versus frequency above 100 Hz (where the resistive contribution is prominent) for *state 0* and *state 1*.

References Supporting Information:

[1] Chidsey, C. E. D.; Bertozzi, C. R.; Putvinski, T. M.; Mujsce, A. M. *J. Am. Chem. Soc.*. **1990**, *112*, 4301

ChemPubSoc Europe

DOI: 10.1002/cphc.201600176

CHEMPHYSCHEM Communications

Special Issue

Donor/Acceptor Mixed Self-Assembled Monolayers for Realising a Multi-Redox-State Surface

Javier Casado-Montenegro, Elena Marchante, Núria Crivillers, Concepció Rovira, and Marta Mas-Torrent*[a]

Mixed molecular self-assembled monolayers (SAMs) on gold, based on two types of electroactive molecules, that is, electron-donor (ferrocene) and electron-acceptor (anthraquinone) molecules, are prepared as an approach to realise surfaces exhibiting multiple accessible redox states. The SAMs are investigated in different electrolyte media. The nature of these media has a strong impact on the types of redox processes that take place and on the redox potentials. Under optimised conditions, surfaces with three redox states are achieved. Such states are accessible in a relatively narrow potential window in which the SAMs on gold are stable. This communication elucidates the key challenges in fabricating bicomponent SAMs as electrochemical switches.

Through the last few decades, the preparation and exploitation of functional self-assembled monolayers (SAMs) have been a topic of intense research, since they have shown appealing properties for a wide range of applications, such as interface engineering in electronic devices,[1] sensing interfaces[2] and molecular switches and motors.[3] A particular approach in the field of molecular electronics is the use of electroactive SAMs to fabricate charge-storage molecular memories in which the different accessible redox states act as memory bits.[4,5] Typically, these systems are composed of a single electroactive unit that can switch between two redox states.[6] The processing of higher memory densities in such devices could be achieved by increasing the number of memory states in each cell.[7] This can be realised by preparing SAMs with molecules that contain two or more electroactive moieties, although their synthesis can be quite complex.[8] An alternative route is to employ molecules that exhibit multiple redox states.[9–11] However, to read all these states it is commonly necessary to apply relatively high voltage potentials, which are in detrimental to SAM stability. Indeed, the application of high voltages to molecularly functionalised gold surfaces through S–Au bonds leads to electrochemical molecular desorption.[12] Hence, the design of hybrid systems (organic molecule/metal electrode) that can operate in a narrow bias window is crucial. Inspired by some recent works on mixed SAMs composed of electron-donor (D) and electron-acceptor (A) units designed to act as artificial systems for light harvesting and energy transfer,[13–17] we have prepared bicomponent mixed SAMs on gold composed of two redox-active species that can be electrochemically switched to achieve a ternary memory that operates in a quite narrow voltage window. In particular, we employ ferrocene (Fc) as D unit and an anthraquinone (AQ) as A unit.

Specifically, the molecules used in this study are 1) the commercially available 11-(ferrocenyl)undecanethiol (**1**), which has a terminal thiol group for grafting to gold and can undergo one reversible oxidation process ($Fc \rightleftarrows Fc^+$), and 2) the anthraquinone derivative **2**, which has a thioctic ester group bearing a disulfide that can react with gold. Generally, AQs exhibit two one-electron redox processes ($AQ \rightleftarrows AQ^{\bullet -} \rightleftarrows AQ^{2-}$) in aprotic media and a single two-proton, two-electron reduction process ($AQ + 2H^+ + 2e^- \rightleftarrows AQH_2$) in protic environments (Figure 1 a).[18] As depicted in Scheme 1, compound **2** is obtained by an esterification reaction between 2-hydroxyanthraquinone (**3**) and α-lipoic acid (**4**); for details of the synthesis and characterisation, see the Supporting Information.

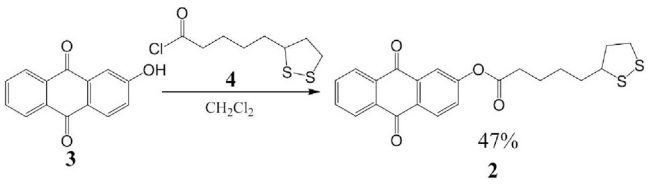

Scheme 1. Synthetic route to **2**.

Cyclic voltammetry (CV) has been used as a tool to characterise the electrochemical properties of electroactive SAMs and the redox-accessible states shown in Figure 1. The type of solvent and the nature and size of the electrolyte ions have a strong influence on the CV response and hence on the performance of the electrochemical switch. Therefore, the optimum CV conditions can vary significantly depending on the electroactive system under examination. A clearly identified challenge here was to find electrolyte media suitable for switching and stabilising the different redox states of the prepared bicomponent SAMs. For this purpose, three different electrolyte solutions were explored in this study: 1) an inorganic salt dissolved in an organic solvent, 2) an aqueous phos-

[a] Dr. J. Casado-Montenegro, E. Marchante, Dr. N. Crivillers, Prof. C. Rovira, Dr. M. Mas-Torrent
Department of Molecular Nanoscience and Organic Materials
Institut de Ciència de Materials de Barcelona (ICMAB-CSIC) and Networking Research Center on Bioengineering, Biomaterials and Nanomedicine (CIBER-BBN)
Campus de la UAB, 08193 Bellaterra (Spain)
E-mail: mmas@icmab.es

Supporting Information for this article can be found under http://dx.doi.org/10.1002/cphc.201600176.

An invited contribution to a Special Issue on Molecular Machines

© 2016 Wiley-VCH Verlag GmbH & Co. KGaA, Weinheim

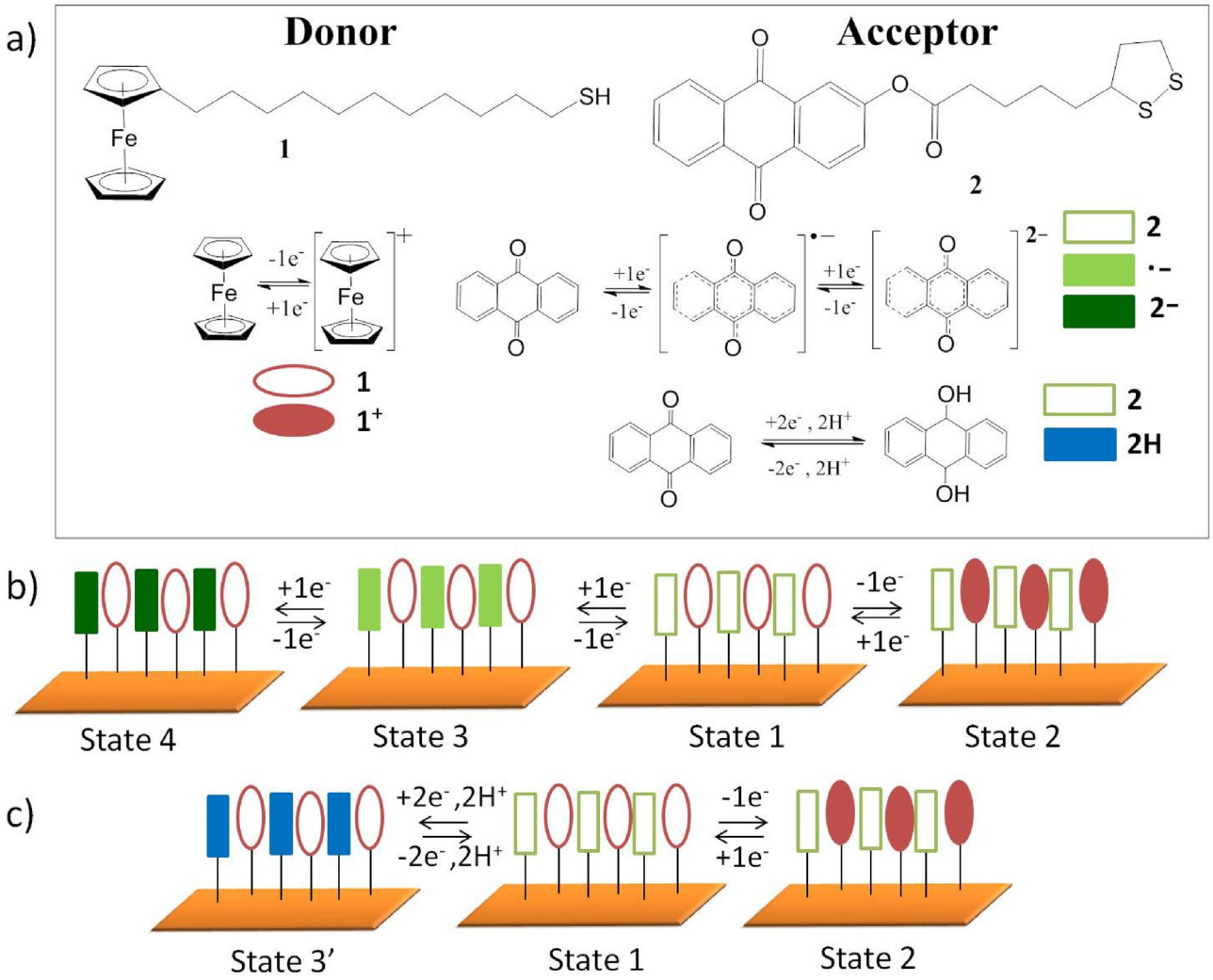

Figure 1. a) Molecular structures of Fc donor **1** and AQ acceptor **2** employed in this study. The colour code for the different redox states is shown. Scheme of the redox processes that could take place on a mixed Fc/AQ SAM on Au employing b) an aprotic or c) a protic medium as electrolyte.

phate buffer solution and 3) an ionic liquid (IL). Electrolytes (1) and (2) have been extensively employed for characterising electroactive SAMs. On the contrary, although ILs offer clear advantages for performing electrochemical studies (i.e. low vapour pressure, high thermal stability, high electrical conductivity and large electrochemical window), their use with SAMs has been less explored.

Prior to formation of the Fc/AQ mixed SAMs, the monocomponent monolayers were prepared and characterised. A commercial substrate consisting of a 50 nm polycrystalline gold film evaporated on glass was used for all the experiments described here. First, the SAM based on **2** was prepared by immersing a freshly cleaned Au substrate in a 0.5 mM solution of **2** in THF for 40 h under inert atmosphere at room temperature with exclusion of light. The resulting modified substrate was characterised by polarisation modulation IR reflection absorption spectroscopy (PM-IRRAS), water contact angle (CA) and CV. The PM-IRRAS spectrum shows three stretching bands, two at 1676 and 1591 cm^{-1} corresponding to the carbonyl groups of the anthraquinone core and one at 1760 cm^{-1} corresponding to the ester group (see Supporting Information, Figure S4). The water CA of 83.1±1.3° measured on the functionalised gold is close to those of other reported monolayers exhibiting an exposed phenyl group.[19] Both results indicate good formation of the AQ SAM.

For electrochemical characterisation, we employed a conventional three-electrode setup with the modified gold substrate as the working electrode (with an area of 0.5 cm^2), a platinum wire as counter electrode and a silver wire as quasi-reference electrode. The first approach was to use the most common conventional conditions, that is, a salt dissolved in an organic solvent as the electrolyte solution. For the AQ SAM we combined different solvents (CH_2Cl_2/MeCN (9/1, v/v), MeCN, acetone and THF) with different salts (NBu_4PF_6, NBu_4ClO_4 and $LiClO_4$). Under all tested conditions, the peak corresponding to the first reduction process (RP1; $AQ \rightarrow AQ^{\bullet-}$) was observed between −0.8 and −1 V versus Ag(s), but the second reduction process (RP2; $AQ^{\bullet-} \rightarrow AQ^{2-}$) could not be measured due to the instability of the SAM when the voltage window was extended to more negative potentials. CV in the solution of NBu_4PF_6 in

© 2016 Wiley-VCH Verlag GmbH & Co. KGaA, Weinheim

acetonitrile gave the lowest absolute $E^{1/2}$(RP1) value [−0.8 V vs Ag(s)], and the lowest peak-to-peak potential splitting ($\Delta E_{pp} = E_{cathodic} - E_{anodic} = 0.13$ V at a scan rate (SR) of 0.3 V s^{-1}), which indicate that the reduced state is more accessible and the redox process is more reversible under these conditions.

In electrolyte solutions based on protic solvents, anthraquinones undergo a two-electron reduction process involving two protons that leads to the hydroanthraquinone form: $AQ + 2H^+ + 2e^- \rightleftarrows AQH_2$. This process typically takes place at voltages closer to 0 V than RP1 of AQ in an aprotic medium. Furthermore, it has been shown that the redox behaviour depends on the pH. Nagata et al. studied the electron transfer of a quinone SAM on gold and showed that, on increasing the pH of the solution, the peak potential shifts towards a more negative potential and the peak separation becomes smaller.[20] Taking this into account and in order to optimise the CV response of the herein-described monolayer, we characterised the AQ SAM in phosphate buffer solution at different pH values (5.0, 6.9 and 8.9). The measured $E^{1/2}$ values versus Ag(s) for increasing pH values were −0.31, −0.39 and −0.62 V, respectively, following the trend previously described in the literature. In addition, the ΔE_{pp} value clearly depends on the pH. The ΔE_{pp} value of 0.25 V at pH 5.0 and SR of 0.3 V s^{-1} considerably diminishes to 0.07 and 0.06 V at pH 6.9 and 8.9, respectively. Hence, the buffer solution at neutral pH 6.9 was taken as optimal for the rest of the experiments, since under these conditions the redox process occurs at lower $|E^{1/2}|$ and shows greater reversibility.

The electrochemistry of AQ derivatives has also been previously investigated in ILs.[21,22] In this work, the AQ SAM was characterised by using 1-butyl-3-methylimidazolium trifluoromethanesulfonate ([BMIM]$^+$[OTf]$^-$) as electrolyte. The IL was exhaustively dried prior to use, and the CVs were acquired under nitrogen in a glove box to avoid moisture, which could lead to formation of AQH_2. Interestingly, in the CV of the AQ SAM in [BMIM]$^+$[OTf]$^-$ (Figure 2) the two reduction processes of AQ-SAM can be observed at $E_1^{1/2} = -0.31$ V ($\Delta E_{pp} = 0.27$ V, SR = 0.1 V s^{-1}) and $E_2^{1/2} = -0.61$ V ($\Delta E_{pp} = 0.19$ V, SR = 0.1 V s^{-1}).

The Fc SAM was prepared by immersing the gold substrate in a 1 mM solution of compound **1** in ethanol for 20 h under argon atmosphere at room temperature with exclusion of light. The measured water CA of 78.0 ± 3.4° is in accordance with previously reported values for similar Fc SAMs.[23] For the Fc SAM, exhaustive electrochemical characterisation was carried out in the optimised electrolytes found for the above-described AQ SAM, that is, MeCN/NBu_4PF_6, [BMIM]$^+$[OTf]$^-$ and buffer solution (pH 6.9). The results showed stable and reproducible CVs with one oxidation wave in the three electrolytic media. The Fc SAM is not stable below −0.8 V versus Ag(s) in ACN/NBu_4PF_6, and therefore this electrolyte was not used for studying the bicomponent monolayer.

Table 1 summarises the $E^{1/2}$ values measured for the AQ SAM and Fc SAM on gold in the three electrolytes. They evidence that the chemical environment has a huge impact on the voltage at which the redox process is observed, and elucidate the importance of correctly choosing the conditions under which a redox-active monolayer is studied, since they can determine the number of states that can be accessed.

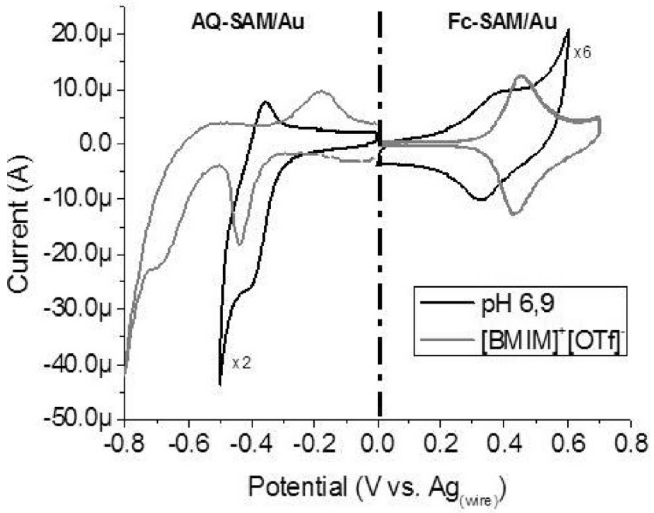

Figure 2. CVs of the monocomponent Fc and AQ SAMs on gold in phosphate buffer solution at pH 6.9 (black) and in [BMIM]$^+$[OTf]$^-$ (grey). Scan rate: 100 mV s^{-1}. The current intensity is scaled for clearer comparison.

Table 1. Values of $E^{1/2}$ [V] versus Ag(s) obtained for the two monocomponent SAMs in different electrolytes.

	MeCN/NBu_4PF_6[a]	Phosphate buffer[b]	[BMIM]$^+$[OTf]$^-$
Fc SAM	+0.41	+0.35	+0.41
AQ SAM	−0.78	−0.39	−0.31, −0.61

[a] 0.1 M. [b] pH 6.9

Figure 2 shows CVs of the two monocomponent SAMs acquired in the electrolytes selected for studying the bicomponent SAMs (i.e. buffer solution at pH 6.9 and [BMIM]$^+$[OTf]$^-$; see Figures S5 and S6 for CVs in ACN/NBu_4PF_6). All the redox processes are observed below |0.8| V vs Ag(s), a voltage window in which the SAMs on gold should be stable. Notably, the AQ reduction peaks clearly shift to lower voltages in the IL.

The mixed SAM was prepared by two approaches: 1) from a mixed-component solution (one step) and 2) sequential immersion in solutions of each component (two steps). To determine the best methodology and to evaluate the reproducibility, the ratio Γ_{AQ}/Γ_{Fc}, where Γ is the surface coverage (see Supporting Information) was used as indicator. The Γ value was extracted from the anodic peak of the Fc oxidation wave and from the cathodic peak of the $AQ \rightleftarrows AQ^{\cdot-}$ process in [BMIM]$^+$[OTf]$^-$ (Table 2). For the one-step procedure a freshly cleaned gold substrate was immersed in a mixed solution of the two compounds (in different molar ratios). This route always led to a very low percentage of AQ linked to the surface. This can be attributed to the strongly preferred adsorption of thiols over disulfides, as previously reported.[24] This is probably due to smaller steric hindrance of thiols on approaching the surface, a lower activation entropy of adsorption or possibly differences in the rates of conversion of the initially physisorbed species to the chemisorbed thiolate.

© 2016 Wiley-VCH Verlag GmbH & Co. KGaA, Weinheim

Table 2. Surface coverages Γ [mol cm^{-2}] calculated for the three mixed SAMs prepared with different immersion times of the AQ SAM in the Fc solution.

Immersion time	Γ_{AQ}	Γ_{Fc}	Γ_{AQ}/Γ_{Fc}
1 h	2.6×10^{-10}	2.6×10^{-11}	10.0
2 h	2.4×10^{-10}	4.9×10^{-11}	5.0
4 h	2.7×10^{-10}	5.2×10^{-11}	5.2

For the two-step procedure, first the freshly cleaned substrate was immersed in a 0.5 mM solution of the AQ **2** in THF for 40 h, and then, the modified substrate was rinsed and immersed in a 1 mM solution of the Fc **1** in THF at room temperature for 1, 2 and 4 h under argon. In all cases good formation of the mixed SAM was observed (see Figure S7). The Γ_{AQ}/Γ_{Fc} ratio decreased from 10.0 to 5.0 on increasing the immersion time from 1 to 2 h, but no significant further decrease occurred when the immersion time was increased to 4 h. Hence, 2 h was established as the most suitable incubation time for the functionalisation with Fc in the preparation of the bicomponent SAM. For comparison, the surface coverages of the monocomponent SAMs were calculated to be $\Gamma_{AQ}=2.8\times10^{-10}$ mol cm^{-2} and $\Gamma_{Fc}=4.0\times10^{-10}$mol cm^{-2}.

The D/A bicomponent SAM was also characterised by X-ray photoelectron spectroscopy, which confirmed the presence of S 2p, Fe 2p and O 1s (for spectra and assignments, see Figure S8).

Cyclic voltammetry allowed the different accessible redox states in the D/A mixed SAM to be identified. States 1, 2 and 3′ (see Figure 1b and c) were electrochemically accessed by using the phosphate buffer (pH 6.9, Figure 3a), and states 1, 2 and 3 by employing [BMIM]$^+$[OTf]$^-$ (Figure 3b). In both cases, we succeeded in realising a SAM-based molecular ternary switch in a voltage window within $\pm$0.8 V versus Ag(s), which is a voltage window in which SAMs are stable. Several consecutive voltage-sweeping cycles were acquired in both electrolytes without showing a significant decrease of the current intensity in the CVs, which revealed that the SAMs are stable (see Figure S9). As shown in Figure 3, the AQ reduction potentials show shifts towards more negative values in both electrolytes compared to the AQ monocomponent monolayer, which could be attributed to the different chemical environments. For this reason, state 4 in Figure 1b corresponding to coexistence of the dianionic form of AQ with the neutral ferrocene species (AQ^{2-}/Fc) was not possible to achieve due to desorption of the grafted Fc molecules at the voltage required for the reduction of $AQ^{\bullet-}$ to AQ^{2-} (see Figure S10).

In summary, a mixed D/A SAM was successfully prepared to achieve a three-state redox molecular switch in a relatively narrow voltage window in which SAMs are stable. It was demonstrated in detail that the choice of electrolyte medium can determine the potential at which the redox processes occur and hence the operational voltage range of the switch. Therefore, this work clearly elucidates the challenges for achieving long-term stable molecular multistate switches by employing multiple redox-active centres covalently linked to a gold surface.

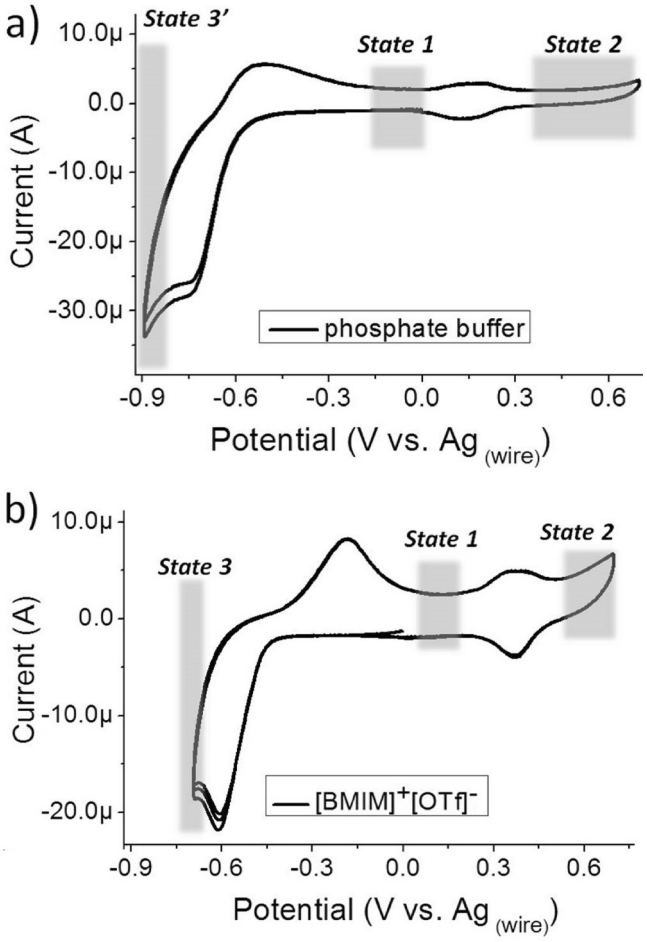

Figure 3. CV of the mixed AQ/Fc SAM on gold in a) phosphate buffer (pH 6.9) and b) [BMIM]$^+$[OTf]$^-$. Scan rate: 100 mV s^{-1}. The shaded areas indicate the different accessed states (see Figure 1).

Acknowledgements

We acknowledge the financial support of the EU projects ERC StG 2012-306826 e-GAMES, ITN iSwitch (GA no. 642196) CIG (PCIG10-GA-2011-303989), ACMOL (GA no. 618082), the Networking Research Center of Bioengineering, Biomaterials and Nanomedicine (CIBER-BBN), the DGI (Spain) with project BE-WELL CTQ2013-40480-R and the Generalitat de Catalunya with project 2014-SGR-17. The authors also acknowledge financial support from the Spanish Ministry of Economy and Competitiveness, through the "Severo Ochoa" Programme for Centres of Excellence in R&D (SEV-2015-0496). N.C acknowledges the RyC Program. J.C-M. and E.M. are enrolled in the Materials Science PhD program of UAB.

Keywords: donor–acceptor systems · electrochemistry · molecular devices · monolayers · self-assembly

© 2016 Wiley-VCH Verlag GmbH & Co. KGaA, Weinheim

[1] H. Ma, H.-L. Yip, F. Huang, A. K.-Y. Jen, *Adv. Funct. Mater.* **2010**, *20*, 1371 – 1388.
[2] J. J. Gooding, F. Mearns, W. Yang, J. Liu, *Electroanalysis* **2003**, *15*, 81 – 96.
[3] B. K. Pathem, S. A. Claridge, Y. B. Zheng, P. S. Weiss, *Annu. Rev. Phys. Chem.* **2013**, *64*, 605 – 630.
[4] Q. Li, G. Mathur, S. Gowda, S. Surthi, Q. Zhao, L. Yu, J. S. Lindsey, D. F. Bocian, V. Misra, *Adv. Mater.* **2004**, *16*, 133 – 137.
[5] Z. Liu, A. A. Yasseri, J. S. Lindsey, D. F. Bocian, *Science* **2003**, *302*, 1543 – 1545.
[6] T. Gupta, M. E. van der Boom, *Angew. Chem. Int. Ed.* **2008**, *47*, 5322 – 5326; *Angew. Chem.* **2008**, *120*, 5402 – 5406.
[7] M. Mas-Torrent, C. Rovira, J. Veciana, *Adv. Mater.* **2013**, *25*, 462 – 468.
[8] L. Y. Wei, K. Padmaja, W. J. Youngblood, A. B. Lysenko, J. S. Lindsey, D. F. Bocian, *J. Org. Chem.* **2004**, *69*, 1461 – 1469.
[9] J. Casado-Montenegro, M. Mas-Torrent, F. Otón, N. Crivillers, J. Veciana, C. Rovira, *Chem. Commun.* **2013**, *49*, 8084.
[10] K. M. Roth, J. S. Lindsey, D. F. Bocian, W. G. Kuhr, *Langmuir* **2002**, *18*, 4030 – 4040.
[11] C. Simão, M. Mas-Torrent, J. Casado-Montenegro, F. Otón, J. Veciana, C. Rovira, *J. Am. Chem. Soc.* **2011**, *133*, 13256 – 13259.
[12] M. Tencer, P. Berini, *Langmuir* **2008**, *24*, 12097 – 12101.
[13] F. Lü, Y. Fang, G. J. Blanchard, *Langmuir* **2008**, *24*, 8752 – 8759.
[14] A. C. Coleman, J. Areephong, J. Vicario, A. Meetsma, W. R. Browne, B. L. Feringa, *Angew. Chem. Int. Ed.* **2010**, *49*, 6580 – 6584; *Angew. Chem.* **2010**, *122*, 6730 – 6734.
[15] H. Imahori, H. Norieda, H. Yamada, Y. Nishimura, I. Yamazaki, Y. Sakata, S. Fukuzumi, *J. Am. Chem. Soc.* **2001**, *123*, 100 – 110.
[16] E. J. Pacsial, D. Alexander, R. J. Alvarado, M. Tomasulo, F. M. Raymo, *J Phys Chem. B* **2004**, *108*, 19307 – 19313.
[17] K. Stranius, L. George, A. Efimov, T.-P. Ruoko, J. Pohjola, N. V. Tkachenko, *Langmuir* **2015**, *31*, 944 – 952.
[18] P. S. Guin, S. Das, P. C. Mandal, *Int. J. Electrochem. Sci.* **2011**, *2011*, 1 – 22.
[19] C. A. Hacker, J. D. Batteas, J. C. Garno, M. Marquez, C. A. Richter, L. J. Richter, R. D. van Zee, C. D. Zangmeister, *Langmuir* **2004**, *20*, 6195 – 6205.
[20] M. Nagata, M. Kondo, Y. Suemori, T. Ochiai, T. Dewa, T. Ohtsuka, M. Nango, *Colloids Surf. B* **2008**, *64*, 16 – 21.
[21] S. Ernst, L. Aldous, R. G. Compton, *Chem. Phys. Lett.* **2011**, *511*, 461 – 465.
[22] V. A. Nikitina, R. R. Nazmutdinov, G. A. Tsirlina, *J. Phys. Chem. B* **2011**, *115*, 668 – 677.
[23] T. Ichii, S. I. Nanjo, K. Murase, H. Sugimura, *Jpn. J. Appl. Phys.* **2009**, *48*, 2 – 5.
[24] C. D. Bain, H. A. Biebuyck, G. M. Whitesides, *Langmuir* **1989**, *5*, 723 – 727.

Manuscript received: February 19, 2016
Accepted Article published: March 27, 2016
Final Article published: April 23, 2016

© 2016 Wiley-VCH Verlag GmbH & Co. KGaA, Weinheim

CHEMPHYSCHEM

Supporting Information

Donor/Acceptor Mixed Self-Assembled Monolayers for Realising a Multi-Redox-State Surface

Javier Casado-Montenegro, Elena Marchante, Núria Crivillers, Concepció Rovira, and Marta Mas-Torrent*[a]

cphc_201600176_sm_miscellaneous_information.pdf

Synthesis of compound **2**:

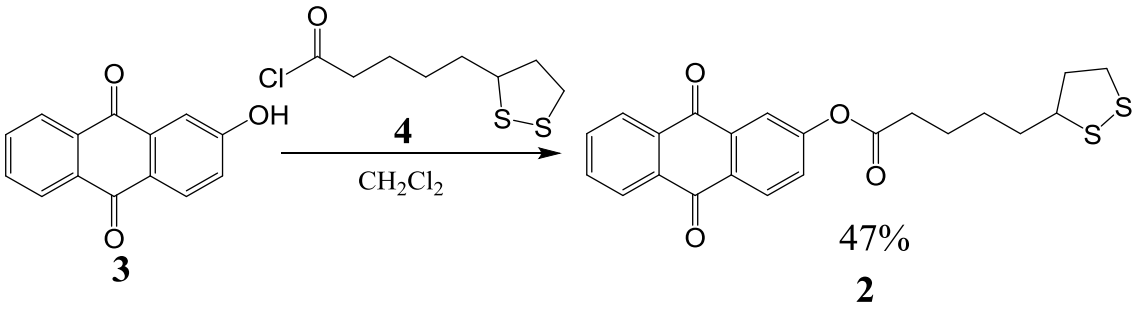

3 **2**

Compound **3** (0.205g 0.915 mmol) is dissolved in dry CH_2Cl_2 (60 ml) and NEt_3 (0.2 ml, 1.49 mmol) is added dropwise. The mixture is stirred at 0°C for 15 min. under Ar atmosphere. After addition of α-lipoic acid chloride (**4**) [1] (0.272g, 1.20 mmol), dissolved in dry CH_2Cl_2 (4 ml) the mixture is stirred overnight at room temperature and the residue purified by a chromatography column (silicagel, CH_2Cl_2) giving **2** (0.158 g, 47%) as a yellow powder. M.P. = 96 - 100°C; ^{1}H-NMR (600 MHz, CD_2Cl_2) δ (ppm): 8.29-8.22 (m, 3H, Ar-H), 7.94 (d, 1H, Ar-H, J=6 Hz), 7.79-7.77 (m, 2H, Ar-H), 7.51-7.49 (m, 1H, Ar-H), 3.62-3.59 (m, 1H), 3.18-3.10 (m, 2H), 2.64 (t, 2H, J = 6 Hz), 2.40-2.34 (m, 1H), 1.94-1.90 (m, 1 H), 1.81-1.70 (m, 4H), 1.59-1.43 (m, 2H); ^{13}C-NMR (150 MHz, CD_2Cl_2) δ (ppm): 182.7 (C=O AQ), 182.4,(C=O AQ), 172.8 (C=O ester), 155.9, 135.6-120.4 (C-Ar), 56.9, 40.1, 39.1, 35.1, 34.6, 29.2, 25.0; FT-IR (ν_{max}, cm^{-1}): 2929, 2850, 1749, 1669, 1588, 1570, 1485, 1459, 1426, 1410, 1380, 1327, 1290, 1213, 1202, 1149, 1122, 932; MALDI-TOF (neg) MS: Calcd. 412.080, Found: 412.215; UV (THF) (λ/nm (logε)): 255 (3,97), 323 (3,00); CV (0.1 M NBu_4PF_6 in CH_2Cl_2:ACN (9:1) *vs*. Fc): one reversible wave corresponding to the AQ to $AQ^{\cdot-}$ process at $E_1^{1/2}$= -1.33 V. Elemental Analysis: Calcd. C, 64.05; H, 4.89; S, 15.55, Found: C, 64.67; H, 5.22; S, 15.16.

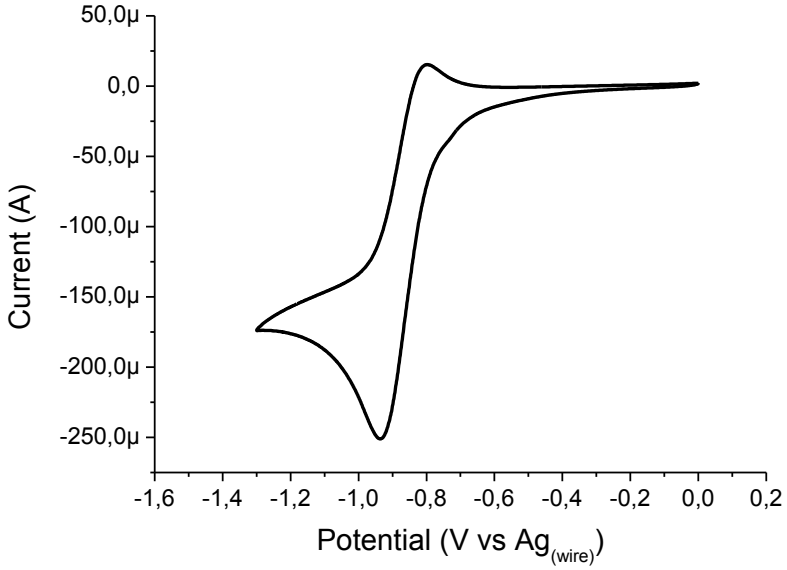

Figure S1. Cyclic voltammetry of the anthraquinone **2** using the Pt wire as the working electrode *vs* Ag(s) and a Pt wire as the counter electrode in 0.1 M NBu_4PF_6 in a mixture dichloromethane:acetonitrile at scan rate 300 mV/s.

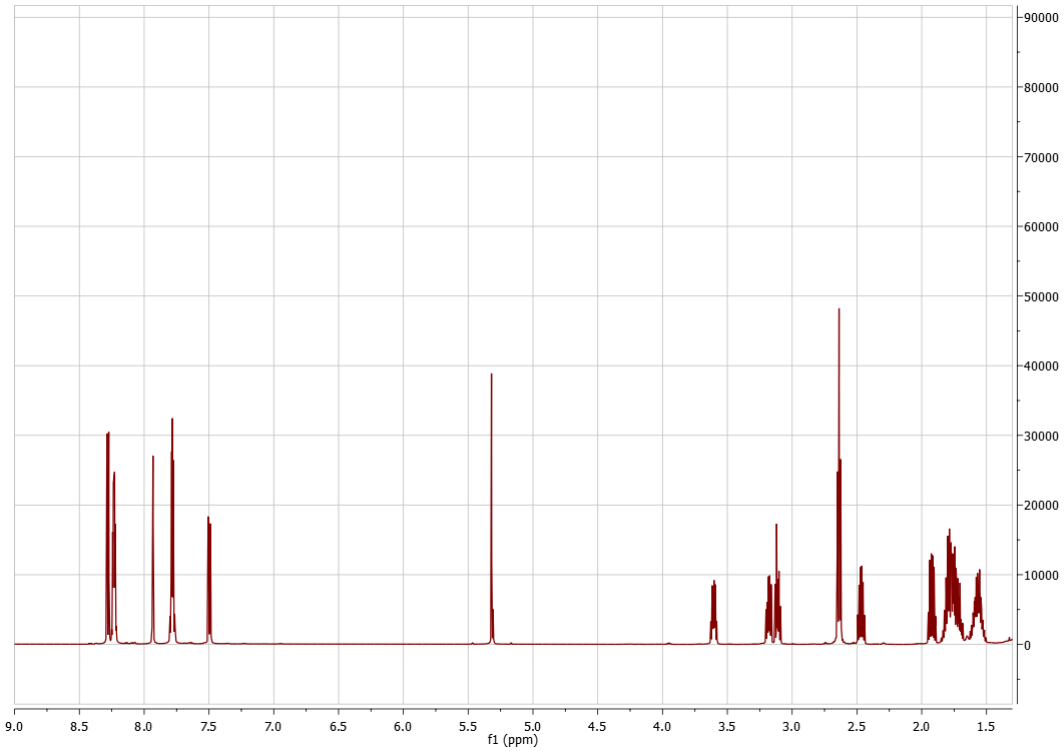

Figure S2. ^{1}H-NMR spectrum in CD_2Cl_2 of the anthraquinone **2**.

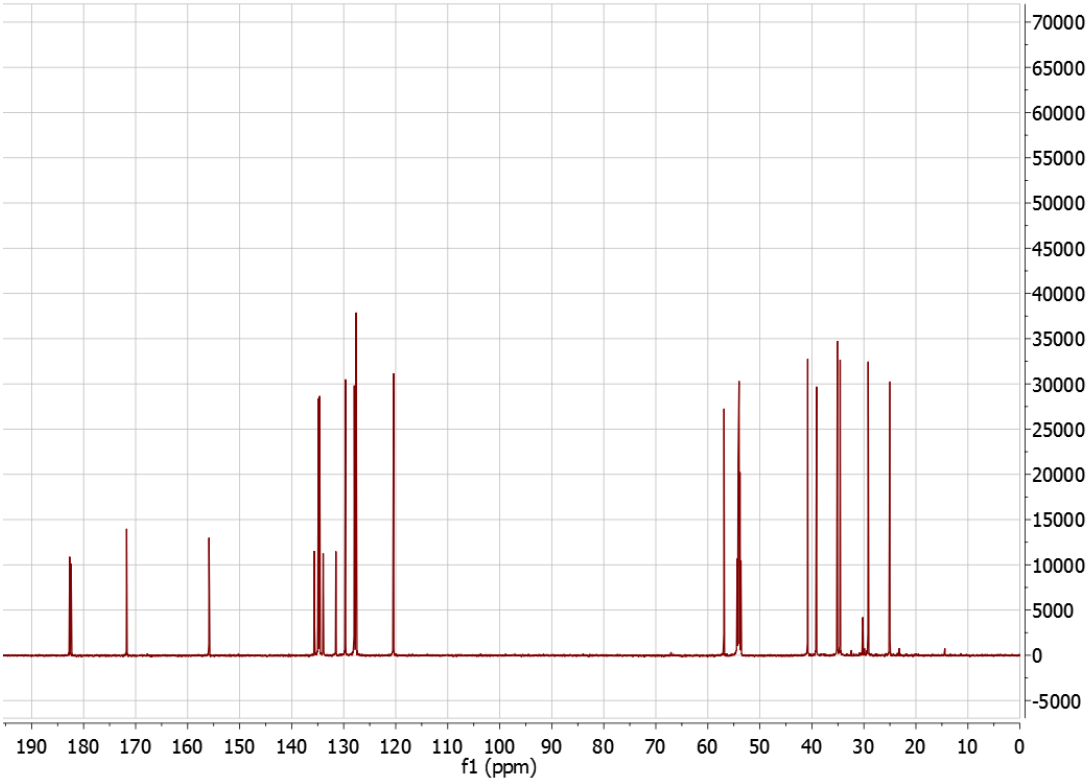

Figure S3. ^{13}C-NMR spectrum in CD_2Cl_2 of the anthraquinone **2**.

General procedure

The ionic liquid used in the study is the 11-Butyl-3-methylimidazolium trifluoromethanesulfonate ($[BMIM]^+[OTf]^-$) purchased from Aldrich

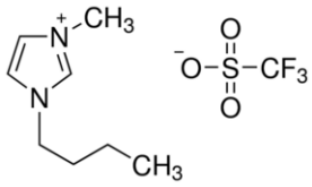

To remove water contamination, it was dried by sparging nitrogen through the RTIL while heating at 100ºC for 2 hours, [2] and then it was immediately placed over a dry molecular sieves and kept in the glove box under nitrogen.

Au substrates consisting of 50 nm of Au on glass were purchased from Phasis.

The phosphate buffer solution was prepared by adjusting the pH to 6.9 adding NaOH to a 250 mM solution of NaH_2PO_4 in ultrapure water.

Cyclic voltammetry experiments were performed using a Novocontrol modular measurement system which consists on an Alpha-AN impedance analyzer equipped with a POT/GAL 30V/2A electrochemical interface. All electrochemical experiments were performed inside the glove box (N_2, H_2O concentration: <1 ppm (20°C, 1 atm); Oxygen concentration: <1 ppm (20°C, 1 atm). A conventional three electrode set-up was employed using the modified gold substrate as the working electrode, a platinum wire as counter electrode and a silver wire as quasi-reference electrode.

We have used a homemade electrochemical cell with a control active area of the functionalized substrate (i.e. working electrode) of 0.5 cm^2.

Contact angle measurements were carried out by using System DSA 100 from KRÜSS. The DSA100 is equipped with software for measuring the contact angle and surface tension of a liquid. Moreover, the contact angle experiments were carried out with 3 microliters of ultrapure water keeping high reproducibility between the replicas due to the automatic dispenser.

PM-IRRAS experiments were performed by using the IR-Spectrometer Vertex 70 from Bruker. The experiments were performed in a sample compartment purged with nitrogen to reduce atmospheric interferents (angle of incidence 80º, spectra collection for 5 min).

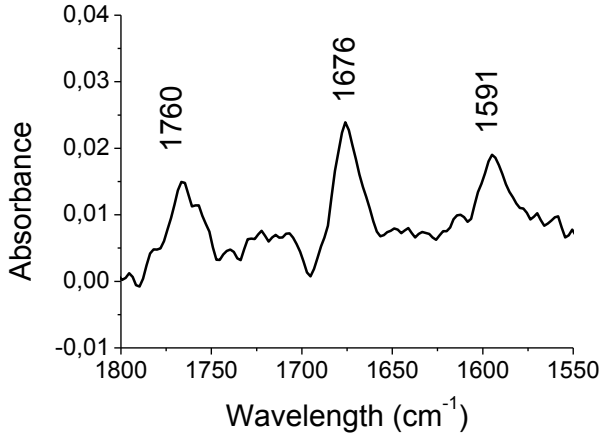

Figure S4. PM-IRRAS spectrum of the mono-component AQ-SAM on gold.

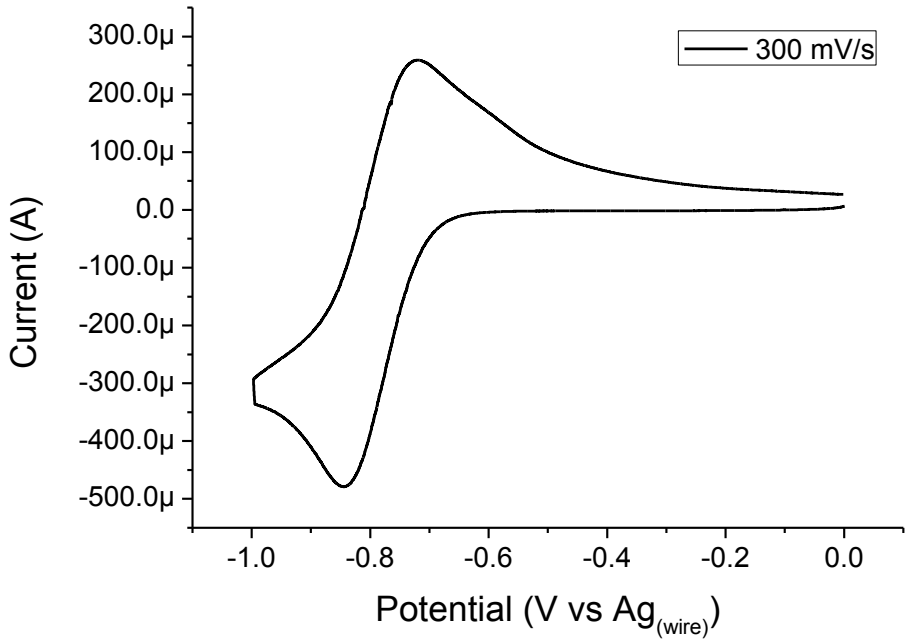

Figure S5. Cyclic voltammetry of the AQ SAM on gold as working electrode vs. Ag(s) and a Pt wire as the counter electrode in 0.1 M NBu_4PF_6 in acetonitrile at 300 mV/s.

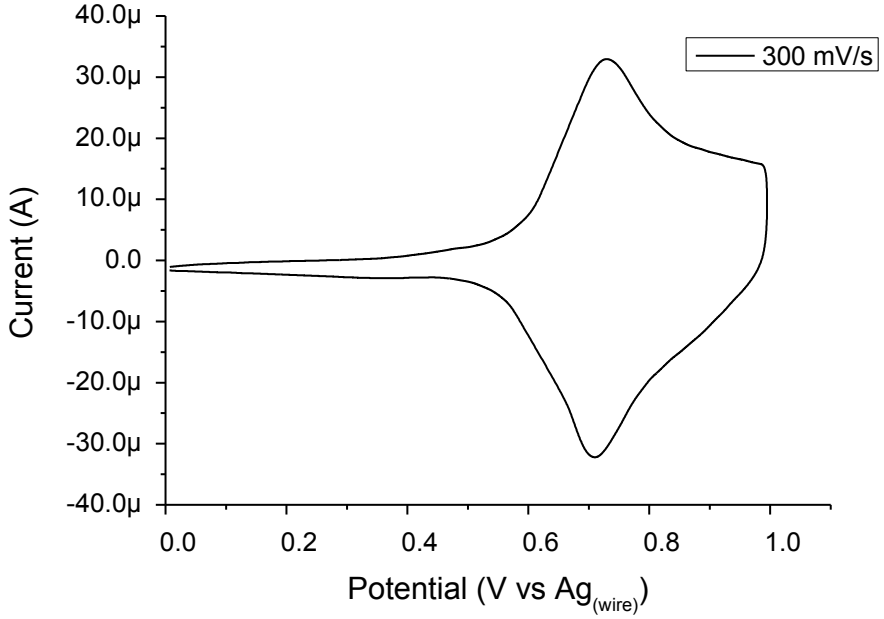

Figure S6. Cyclic voltammetry of the Fc SAM on gold as working electrode vs. Ag(s) and a Pt wire as the counter electrode in 0.1 M NBu_4PF_6 in acetonitrile at 300mV/s.

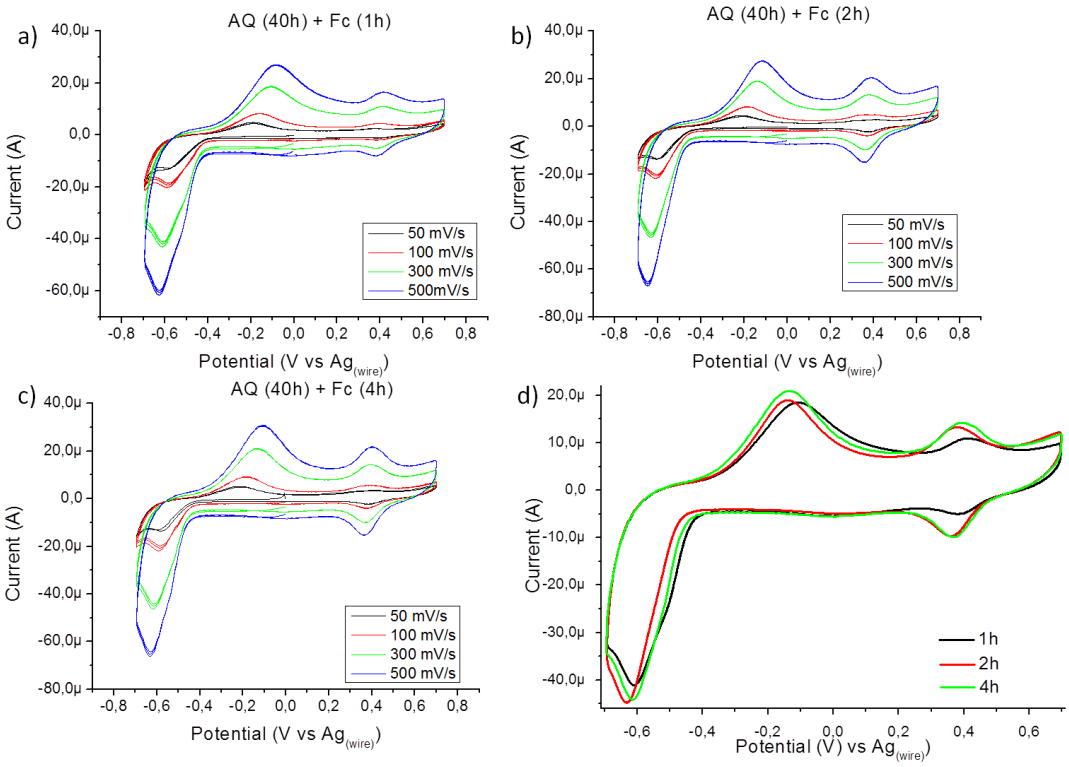

Figure S7. Cyclic voltammograms of three different Fc/AQ mixed-SAMs prepared following the two steps methodology. 1st preparation of the AQ-SAM on Au (40h immersion) and 2nd immersion of the AQ-SAM on Au in the Fc solution for: 1h (a), 2h (b) and 4h (c). Electrolyte: $[BMIM]^+[OTf]^-$, Pt wire as counter and Ag wire as pseudo-reference electrodes. CVs were acquired at the different scan rates indicated in the legend. d) Overlap of the different CVs at the same scan rate (300 mV/s).

The **surface coverage** was obtained from the conventional equation: $\Gamma = Q/nFA$

where Γ is the surface concentrations in mol cm^{-2}, Q is the integrated area of the anodic or cathodic charge, n is the number of electrons transferred (n=1), F is Faraday's constant, and A is the electrode surface area.

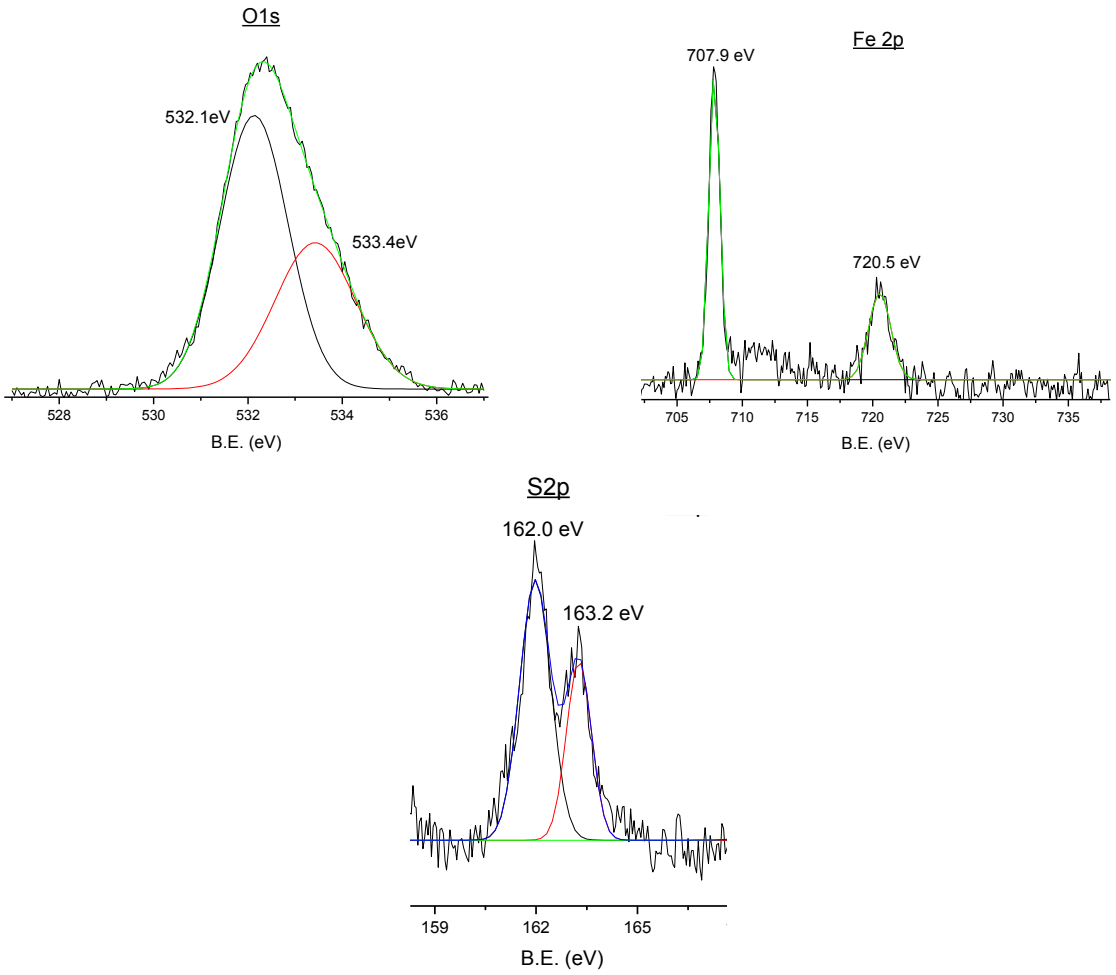

Figure S8. High-resolution XPS of O1s, Fe2p and S2p spectra from the optimized mixed SAM AQ/Fc.

The S2p peaks were fitted using doublet peaks with $2p_{1/2}$/ $2p_{3/2}$ ratio of 0.5 and separation of 1.2 eV, as previously reported. The doublet at 162 eV is attributed to the Au-thiolated species. A doublet located at 707.9 eV and 720.eV corresponding to the Fe $2p_{3/2}$ and Fe $2p_{1/2}$ demonstrates the presence of the Fc molecules in agreement with previous works [3]. The O 1s spectrum shows a peak with contribution of two peaks at 532.0 eV and 532.8 eV that could be attributed to the C-O of the ester and the C=O of the carbonyl groups present in the AQ core. These results support the presence of both species AQ and Fc on the gold surface as electrochemically observed.

a)

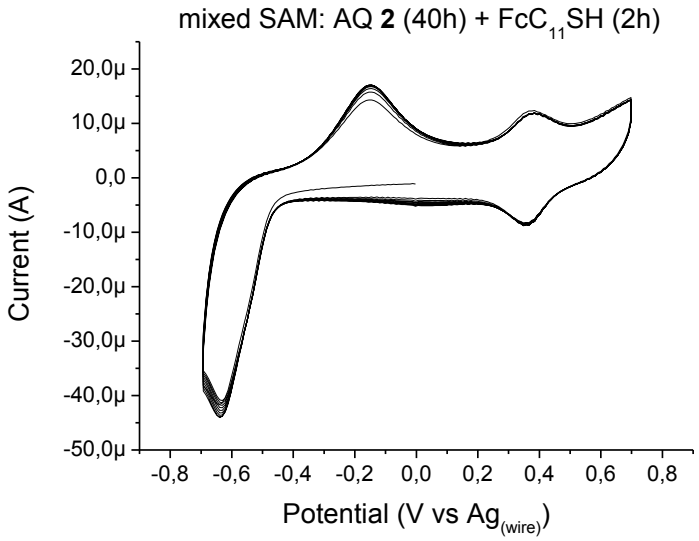

b)

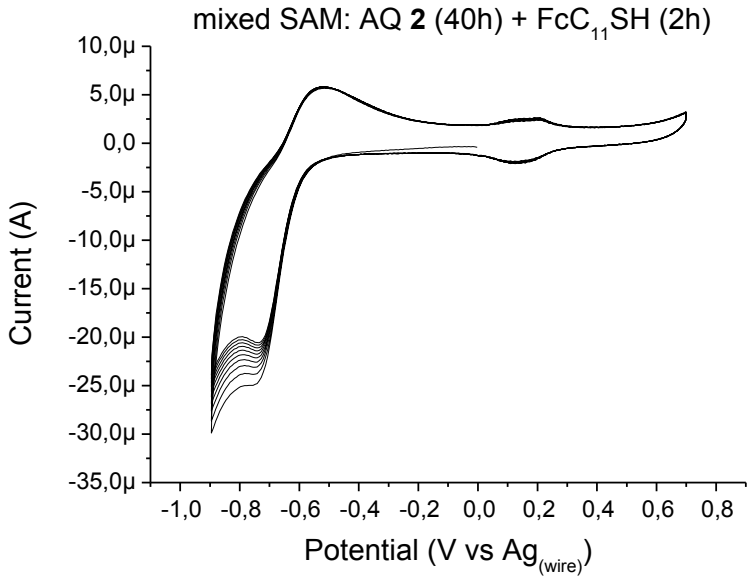

Figure S9. CVs of the bi-component SAMs in a) the ionic liquid $[BMIM]^+[OTf]^-$ (SR=300 mV/s), and b) the phosphate buffer solution (pH=6.9) (SR=100 mV/s). In both cases 10 consecutives voltage sweeping cycles were acquired to corroborate the stability of the SAM. In b) there is a slight variation of the intensity of the AQ redox peak which is stabilized after several cycles. Pt wire and Ag wire are used as counter- and pseudo-reference electrodes, respectively.

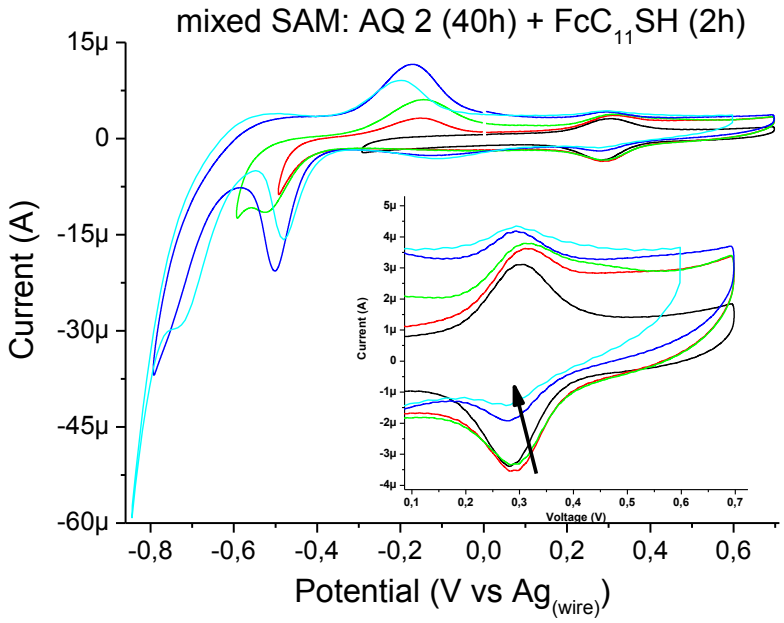

Figure S10. Cyclic voltammetry of the Fc/AQ mixed-SAM/Au, prepared by immersion of the AQ-SAM on Au in the Fc solution for 2h. In the inset figure is shown that the current intensity corresponding to the Fc redox peak decreases when the negative voltage limit is brought below -0.6V (blue and cyan curves). That means that the Fc molecules are being desorbed from the surface. Electrolyte: $[BMIM]^+[OTf]^-$, Pt wire as counter and Ag wire as pseudo-reference electrodes.

[1] M. Gelo-Pujic, J. R. Desmurs, S. Delaire, A. Adao, D. Tawil, *Int. J. Cosmet. Sci.* **2008**, 30, 195.

[2] R. Jarasova, G. M. Swain, *Journal of The Electrochemical Society*, **2015**, *162*, H507-H511.

[3] C. M. Woodbridge, D. L. Pugmire, R. C. Johnson, N. M. Boag and M. A. Langell, *J. Phys. Chem. B*, **2000**, 104, 3085.

RSC Advances

PAPER

View Article Online
View Journal | View Issue

CrossMark click for updates

Cite this: *RSC Adv.*, 2017, **7**, 5636

A four-state capacitance molecular switch based on a redox active tetrathiafulvalene self-assembled monolayer†

E. Marchante, M. S. Maglione, N. Crivillers, C. Rovira and M. Mas-Torrent*

Received 18th November 2016
Accepted 29th December 2016

DOI: 10.1039/c6ra27011e

www.rsc.org/advances

An electroactive tetrathiafulvalene (TTF) self-assembled monolayer (SAM) on gold has been prepared and fully characterised by electrochemical impedance spectroscopy. Transfer rates of the same order were found for the two redox processes. Remarkably, the TTF SAM was successfully exploited as a 4-state electrochemical switch using the capacitance of the SAM as output signal.

Open Access Article. Published on 17 January 2017. Downloaded on 17/01/2017 14:25:40.
This article is licensed under a Creative Commons Attribution 3.0 Unported Licence.

The development of molecules possessing different reversible redox stable states has attracted great interest for their potential as active units in charge-storage electronic devices.[1–3] Hybrid organic–inorganic materials that consist of the immobilisation of the active molecules on solid supports provide a promising alternative route to existing silicon technology. One example of these hybrid materials consists of the chemical grafting of the functional molecules on conducting surfaces by forming a self-assembled monolayer (SAM).[4] Commonly, redox-active SAMs are composed of a single electroactive unit that can switch between typically two redox states.[5] Such bi-stable systems can hence mimic current memory devices which are based on binary systems where every bit is coded by a 0 or 1, corresponding to a low or high signal.[6–9] However, one approach to deal with the ever-increasing information density, is to increase the number of memory states in each cell. For this purpose, the realization of electroactive surfaces with multiple accessible redox states is highly desirable.[10] Only a few examples of ternary and quaternary redox SAMs can be found in the literature, which have been achieved by employing molecules that exhibit several redox states[11–16] or molecules that contain two electroactive moieties,[17,18] or by preparing bi-component SAMs with two functional molecules.[19] The former strategy is synthetically less demanding, although it is challenging to find electroactive molecules with more than three accessible redox states in a voltage window where the SAMs linked to a substrate are stable. In all these cases each molecular redox state has been attributed to one memory bit. However, it has been previously shown in self-assembled multilayers of an Os^{2+} complex that the definition of the number of states is not limited by the redox bi-stability of this system, but it can be enhanced if at specific input values distinct levels of the output signal can be determined.[12] As a readout signal in these types of electroactive SAMs the optical response (*i.e.*, absorption) has been extensively employed.[5,15,16,20] Nonetheless, the use of electrical signals is particularly appealing since they can be more easily integrated with modern technologies. Recently, we demonstrated in a ferrocene SAM that the capacitance of the SAM before and after the redox peak determined by electrochemical impedance spectroscopy (EIS) can be successfully exploited as output of the electrochemical switch.[21] Here, we carried out a step forward by applying this methodology in a system with more accessible redox states, in particular in a SAM of a tetrathiafulvalene (TTF) derivative on gold. TTFs exhibit two redox processes and are ideal candidates to be applied in molecular switches.[22–25] The TTF SAMs were prepared and fully characterised by EIS in order to determine the two electron transfer constants and the capacitance of the system at different applied voltages. Four different states were defined and the electrochemical switching response was successfully monitored employing the SAM capacitance as a readout mechanism.

The TTF derivative **1** (Fig. 1A) was synthesised following the methodologies reported in the literature (see ESI† for synthetic details).[26–28] This molecule bears a disulfide group that can react with gold surfaces in order to form a covalent bonded SAM. The SAMs were prepared by immersion of the freshly cleaned substrates in a 1 mM solution of **1** in dry THF under an inert atmosphere and room temperature for 72 h. Subsequently, the functionalized samples were rinsed carefully with THF and dried under a stream of nitrogen giving the target TTF-SAM (Fig. 1A). The SAMs were successfully characterised by X-ray Photoelectron Spectroscopy (XPS) and Time-of-Flight Secondary Ion Mass Spectrometry (ToF-SIMS) (Table S1 and Fig. S1 ESI†).

The confinement of the TTF core on the electrode surface provides an electrochemical interface with three stable redox states, *i.e.*, the neutral, the radical cation and the dication forms

Institut de Ciència de Materials de Barcelona (ICMAB-CSIC), Networking Research Center on Bioengineering, Biomaterials and Nanomedicine (CIBER-BBN), Campus de la UAB, 08193 Bellaterra, Spain. E-mail: mmas@icmab.es

† Electronic supplementary information (ESI) available. See DOI: 10.1039/c6ra27011e

This journal is © The Royal Society of Chemistry 2017

Open Access Article. Published on 17 January 2017. Downloaded on 17/01/2017 14:25:40.
This article is licensed under a Creative Commons Attribution 3.0 Unported Licence.

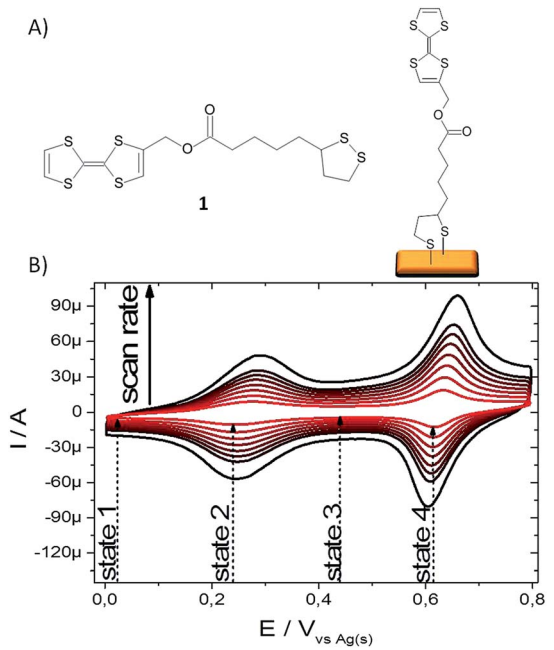

Fig. 1 (A) TTF molecule **1** and scheme of its corresponding SAM on gold. (B) CV of TTF-SAM in $LiClO_4$ 0.1 M in acetonitrile at scan rates 0.1, 0.2, 0.3, 0.4, 0.5, 0.6, 0.7 and 1 V s^{-1}.

of TTF. The TTF-Au modified electrodes were characterized then using electrochemical techniques. Fig. 1B shows the voltammetric response of the TTF-modified Au surface at different potential scan rates (ν) measured using a solution of $LiClO_4$ 0.1 M in acetonitrile as electrolyte, the functionalized surface as working electrode and platinum and silver wires as counter and pseudo-reference electrodes, respectively. Expectedly, two reversible one-electron processes corresponding to the TTF/$TTF^{\cdot+}$ and $TTF^{\cdot+}/TTF^{2+}$ redox couples were observed at the formal potentials $E'_1 = 0.26$ V and $E'_2 = 0.63$ V *vs.* $Ag_{(s)}$ (at a scan rate of 100 mV s^{-1}), respectively. The linear relationship between I_{pa} (*i.e.*, the anodic peak current intensity) and ν is in agreement with the presence of surface-confined redox-active molecules (see ESI, Fig. S2†), along with the small peak-to-peak separations ($\Delta E_p = E_{anodic} - E_{cathodic}$) observed at low scan rates for the two redox processes, $\Delta E_{p1} = 27$ mV and $\Delta E_{p2} = 19$ mV.[29] The full width at half maximum (fwhm) in a theoretical case, where an ideal Nernstian reaction under the Langmuir isotherm conditions (*i.e.*, all adsorption sites are equivalents and there are no interactions between immobilized electroactive centers) occurs at 25 °C, is *ca.* 90 mV.[30] The deviations from the theoretical fwhm value gives hence information about the redox centers, especially related to the intermolecular interactions.[31,32] In this case, the fwhm value of the first redox peak of the TTF-SAMs was larger than 90 mV (*i.e.*, 143 mV), whereas for the second redox peak was slightly lower than the theoretical value (*i.e.*, 79 mV). This type of CV shape has been commonly observed in other TTF-SAMs.[13,33,34] From the area under the cyclic voltammetry peak, the TTF surface coverage was estimated to be 2.2×10^{-10} mol cm^{-2} (at 100 mV s^{-1} of scan rate). Repeated electrochemical cycling demonstrated that the SAM was stable and only a significant reduction in the CV was detected when the potential was scanned beyond the first redox process (Fig. S3†).

Electrochemical impedance spectroscopy (EIS) is a powerful tool to characterize electrical interfacial properties.[35] In SAMs it has mainly been previously employed to determine electron transfer rates in electroactive systems[36] or to investigate the ionic permeability through SAMs based of non-electroactive molecules.[37] To characterise the TTF-SAM, impedance spectra were collected, in the same conditions as the ones used in the CV experiments, between 200 kHz and 500 mHz with an AC amplitude of 5 mV (peak to peak) at three different voltages: before the redox process (10 mV), at the first redox peak potential (250 mV), and at the second redox peak potential (620 mV). Nyquist and Bode plots, shown in Fig. 2A and B, respectively, are the standard diagrams to represent EIS measurements.[38–40] In cases where a DC-current can be established, such as when an ion pair is present in the electrolyte solution, Nyquist plots typically display one or more semicircles.[35] Nevertheless, in the case of surface confined molecules under an inert electrolyte, a DC-current cannot be established, and the system shows capacitor behaviour. Accordingly, the Nyquist plots of the TTF-SAM look like straight vertical lines parallel to the y axis (Fig. 2A).[41–45] The Bode magnitude plots (impedance modulus ($|Z|$) *vs.* frequency) at the low frequency region consist of straight lines with slopes close to -1, while the phase angles (ϕ) approach $-90°$. This behaviour is in agreement with a capacitor-like system,[46] where the gold metal surface acts as one of the capacitor plate and the physisorbed ions at the SAM/electrolyte interface act as the other capacitor plate.[47] At higher frequencies ($f > 10$ kHz), the frequency-independent impedance and phase angle close to zero indicate that the system behaves as a resistor, that is, the total impedance is dominated by the solution resistance.[47] This is due to the fact that at high frequencies, the capacitor behaves as a short-circuit element since there is no time to be charged, allowing the AC current to pass. Noticeable, a significant modulation in $|Z|$ is observed at the low frequency region depending on the DC voltage applied (*i.e.*, on the SAM redox state), indicating that the performed impedance measurements could be successfully used as a readout of the molecular switch. Alternatively, the data can be analyzed by means of capacitance Bode plots by using the expressions:[40,41,48] $C_{re} = -Z_{im}[(j2\pi fZ)^{-1}]$ and $C_{im} = -Z_{re}[(-j2\pi fZ)^{-1}]$, where Z_{re} and Z_{im} are the real and imaginary part of the complex impedance, respectively, and f the frequency.

In fact, capacitance Cole–Cole plots, where the imaginary (C_{im}) *versus* the real (C_{re}) part of the capacitance are represented, provide very useful information for surface confined redox species.[41–45,48–50] Fig. 2C clearly illustrates that different processes with different time constants are occurring depending on the applied DC potential. The small semicircle recorded at a voltage outside the redox process (*i.e.*, 10 mV) comes from the non faradaic terms dominated by the resistance of the electrolyte (R_e) and the double layer capacitance (C_{dl}). In the redox window potentials faradaic contributions are also present (*i.e.*, a pseudo-capacitance for charging the monolayer and a resistance for the electron transfer). Noteworthy, the influence

Open Access Article. Published on 17 January 2017. Downloaded on 17/01/2017 14:25:40.
This article is licensed under a Creative Commons Attribution 3.0 Unported Licence.

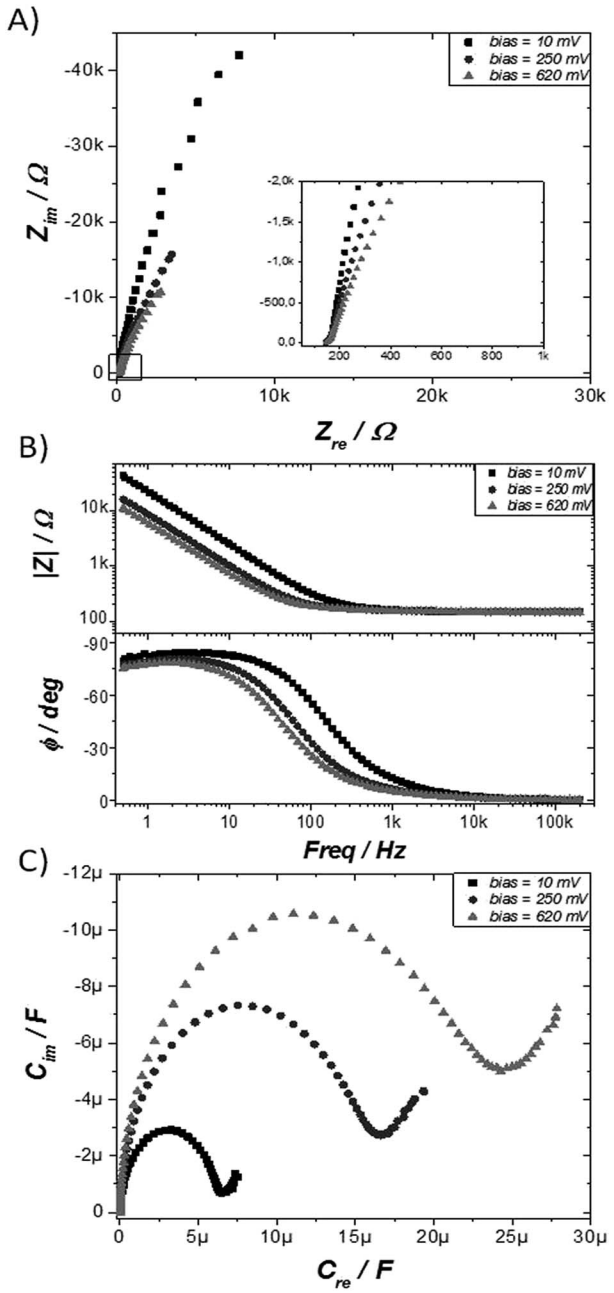

Fig. 2 EIS characterization of TTF-SAM at 3 different bias voltages: 10 mV (■), 250 mV (●), and 620 mV (▲) *vs.* $Ag_{(s)}$. (A) Nyquist plot, (B) Bode plot, and (C) Cole–Cole Plot.

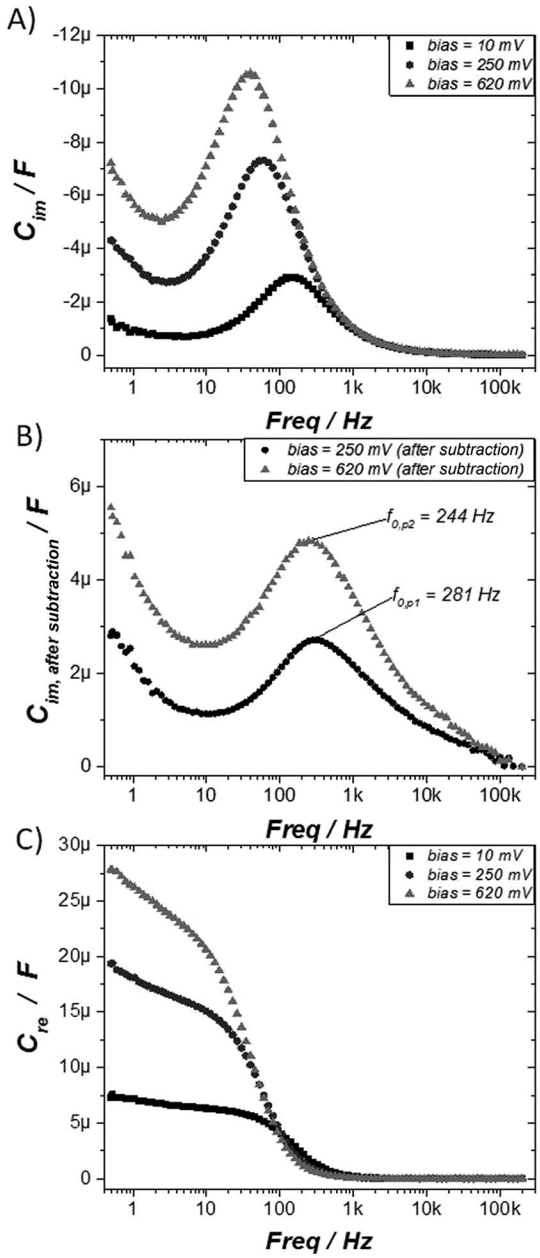

Fig. 3 Capacitance Bode plots of TTF-SAM at 3 different bias voltages: 10 mV (■), 250 mV (●), and 620 mV (▲) *vs.* $Ag_{(s)}$: (A) experimental data of the imaginary part of the capacitance *vs.* frequency, and (B) after subtraction of the non-faradaic response. In (C) is represented the experimental data for the real part of the capacitance *vs.* frequency.

of applied potential on the capacitance spectra of bare Au was much smaller than when the gold is functionalised with the TTF electroactive monolayer, indicating that the observed effect is not simply due to the polarisation of the metal but to the redox processes involved (Fig. S4†).

The imaginary part of the capacitance for the prepared TTF-SAMs is plotted against frequency at DC bias 10, 250 and 620 mV, as shown in Fig. 3A. From this data, it is possible to extract information about the kinetic parameters of the redox transfer.[41–45,48–50] However, first it is necessary to treat the data. First the solution resistance (R_e), which is easily extracted from the beginning of Z_{re} at high frequency in the Nyquist plot, should be subtracted from the spectrum by means of $Z_{re}(f) - R_e$.[48] Then, the blank response from the experimental data registered at 10 mV is also subtracted. In this way, we can gain information exclusively on the redox processes, free of parasitic signals. Fig. 3B shows the final responses of the two C_{im} spectra that correspond to the first and second redox processes, respectively, after the subtraction of the response of the SAM outside the redox window. From these graphs, the rate constant for the electron transfer process (k_{ET}) can be estimated from the frequency (f_0) at the highest ordinate point using the

 This journal is © The Royal Society of Chemistry 2017

Open Access Article. Published on 17 January 2017. Downloaded on 17/01/2017 14:25:40.
This article is licensed under a Creative Commons Attribution 3.0 Unported Licence.

expression: $k_{ET} = \pi f_0$.[41–45,48–50] The k_{ET} values for the TTF/TTF$^{\cdot+}$ and TTF$^{\cdot+}$/TTF^{2+} redox processes were estimated to be 882 and 767 s^{-1}, respectively. Noticeably, previously reported transfer rates for TTF SAMs extracted from applying Laviron's formalism on the CV data gave a higher value for the second oxidation process than for the first one.[51,52] This trend was attributed to environmental effects such as the formation of ion pairs between the oxidized TTF molecules and the electrolyte anions that accelerated the second redox process.[50–52] However, in our study the transfer rates found for the two TTF redox processes by EIS are of the same order.

Further, the C_{re} *versus* frequency plot is illustrated in Fig. 3C. We found that at medium/high frequency range, the measured capacitance corresponds to the bulk capacitance, whereas at low frequency values a plateau is reached reflecting the interfacial double-layer capacitance.[53] Consequently, at this low frequency the capacitance is clearly dependant on the redox state of the molecule and, thus, on the applied DC voltage. Therefore, this result prompted us to investigate the capacitance response in the electrochemical switchable TTF-SAM at low frequency. Taking into account the CV data, four different voltage inputs were selected: 10, 250, 450 and 620 mV *vs.* $Ag_{(s)}$, respectively (Fig. 1B). Such voltages correspond, respectively, to a state where the TTF molecule is in neutral state (state 1), where the first oxidation process occurs (state 2), where all the TTF surface-confined molecules should exist as TTF$^{\cdot+}$ radical-cation (state 3) and the last one where the second oxidation process takes place (state 4). A schematic representation of the different TTF-SAM redox states can be found in Fig. S5.† Hence EIS measurements were performed at 1 Hz at the selected DC potentials. In Fig. 4 evolution of C_{re} in the four states is shown when 20 cycles were applied to the TTF functionalised gold substrate.

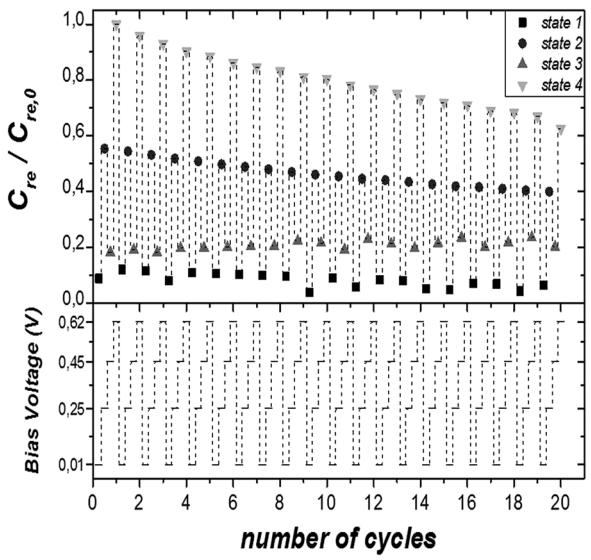

Fig. 4 Four-state switching behavior of TTF-SAM on gold: at the bottom, applied bias voltage profile; at the top, $C_{re}/C_{re,0}$ (at 1 Hz) output at the corresponding states: state 1 (10 mV), state 2 (250 mV), state 3 (450 mV) and state 4 (620 mV).

Capacitance values discernible and specific for each state with significant on/off ratios were found, validating the feasibility of using the SAM capacitance as output of the electrochemical switch. A perceptible decrease of the initial capacitance value of 3, 15, 2 and 30% for states 1–4, respectively, after 20 cycles, was found. As the values indicate, such variation is more pronounced at the states corresponding to the potential of the redox process. This is attributed to some molecular desorption caused by the bias stress. This is also in accordance to the changes observed in the CV of the SAM before and after the impedance switching experiments (Fig. S6†). The switching response was studied in different samples after the application of 50 cycles achieving similar results (Fig. S7†). Therefore, it has been successfully achieved a surface confined molecular switch operating with both and electric input and output signals by making use of the SAM capacitance. It should be highlighted though that the robustness of the system is limited to the electrochemical stability of the sulphur–gold covalent bond which could probably be improved by avoiding extremely traces of humidity and oxygen. We also anticipate that other SAMs such as silane derivatives on ITO would be more durable.[13,19]

Conclusions

In summary, a functionalised gold surface with a TTF derivative was prepared in order to realise a surface with multiple accessible redox states. Such hybrid material was investigated as a four-state surface-immobilized switch by taking advantage of the different capacitance response under the application of external electric fields. Importantly, the number of states of the switch was not limited to the number of redox states of the molecule but instead it was determined by the output of the system at defined DC applied potentials. It should be also noticed that quaternary logic storage platforms can easily match the present binary system as they can be decoded directly into two binary-digit equivalents.[54–56] Complementary, high and comparable values of k_{ET} were obtained by EIS for the two redox process of the TTF. Thus, the results here reported might encourage the development of this type of electrochemical molecular switches for the future implementation in devices.

Acknowledgements

We acknowledge financial support from the EU (projects ERC StG 2012-306826 e-GAMES and ITN iSwitch 642196), the Networking Research Center on Bioengineering, Biomaterials and Nanomedicine (CIBER-BBN), the DGI (Spain) project BE-WELL CTQ2013-40480-R, the Generalitat de Catalunya (2014-SGR-17) and the Spanish Ministry of Economy and Competitiveness, through the "Severo Ochoa" Programme for Centres of Excellence in R&D (SEV-2015-0496). E. M. and M. S. M. are enrolled in the Materials Science PhD program of the UAB.

Open Access Article. Published on 17 January 2017. Downloaded on 17/01/2017 14:25:40.
This article is licensed under a Creative Commons Attribution 3.0 Unported Licence.

References

1 J. R. Heath, J. F. Stoddart, R. S. Williams, E. A. Chandross and P. S. Weiss, *Science*, 2004, **303**, 1137.
2 N. Fuentes, A. Martín-Lasanta, L. Álvarez de Cienfuegos, M. Ribagorda, A. Parra and J. M. Cuerva, *Nanoscale*, 2011, **3**, 4003.
3 F. Meng, Y.-M. Hervault, Q. Shao, B. Hu, L. Norel, S. Rigaut and X. Chen, *Nat. Commun.*, 2014, **5**, 3023.
4 A. Ulman, *Chem. Rev.*, 1996, **96**, 1533–1554.
5 T. Gupta and M. E. Van Der Boom, *Angew. Chem., Int. Ed.*, 2008, **47**, 5322–5326.
6 M. Emmelius, G. Pawlowski and H. W. Vollmann, *Angew. Chem., Int. Ed. Engl.*, 1989, **28**, 1445–1471.
7 S. Kawata and Y. Kawata, *Chem. Rev.*, 2000, **100**, 1777–1788.
8 M. Alexe, C. Harnagea, A. Visinoiu, A. Pignolet, D. Hesse and U. Gösele, *Scr. Mater.*, 2001, **44**, 1175–1179.
9 Q. Zhang, J. He, H. Zhuang, H. Li, N. Li, Q. Xu, D. Chen and J. Lu, *Adv. Funct. Mater.*, 2016, **26**, 146–154.
10 M. Mas-Torrent, C. Rovira and J. Veciana, *Adv. Mater.*, 2013, **25**, 462–468.
11 D. Gryko, J. Li, J. R. Diers, K. M. Roth, D. F. Bocian, W. G. Kuhr and J. S. Lindsey, *J. Mater. Chem.*, 2001, **11**, 1162–1180.
12 G. De Ruiter, L. Motiei, J. Choudhury, N. Oded and M. E. Van Der Boom, *Angew. Chem., Int. Ed.*, 2010, **49**, 4780–4783.
13 C. Simão, M. Mas-Torrent, J. Casado-Montenegro, F. Otón, J. Veciana and C. Rovira, *J. Am. Chem. Soc.*, 2011, **133**, 13256–13259.
14 J. Casado-Montenegro, M. Mas-Torrent, F. Otón, N. Crivillers, J. Veciana and C. Rovira, *Chem. Commun.*, 2013, **49**, 8084–8086.
15 I. Alcón, M. Gonidec, M. R. Ajayakumar, M. Mas-Torrent and J. Veciana, *Chem. Sci.*, 2016, **7**, 4940–4944.
16 A. Kumar, M. Chhatwal, P. C. Mondal, V. Singh, A. K. Singh, D. a. Cristaldi, R. D. Gupta and A. Gulino, *Chem. Commun.*, 2014, **50**, 3783–3785.
17 L. Wei, K. Padmaja, W. J. Youngblood, A. B. Lysenko, J. S. Lindsey and D. F. Bocian, *J. Org. Chem.*, 2004, **69**, 1461–1469.
18 C. Simao, M. Mas-Torrent, V. André, M. T. Duarte, J. Veciana and C. Rovira, *Chem. Sci.*, 2013, **4**, 307–310.
19 J. Casado-Montenegro, E. Marchante, N. Crivillers, C. Rovira and M. Mas-Torrent, *ChemPhysChem*, 2016, **17**, 1810–1814.
20 C. Simão, M. Mas-Torrent, N. Crivillers, V. Lloveras, J. M. Artés, P. Gorostiza, J. Veciana and C. Rovira, *Nat. Chem.*, 2011, **3**, 359–364.
21 E. Marchante, N. Crivillers, M. Buhl, J. Veciana and M. Mas-Torrent, *Angew. Chem., Int. Ed.*, 2016, **55**, 368–372.
22 D. Canevet, M. Sallé, G. Zhang, D. Zhang and D. Zhu, *Chem. Commun.*, 2009, **7345**, 2245–2269.
23 P. Batail, *Chem. Rev.*, 2004, **104**, 4887–4890.
24 J. L. Segura and N. Martn, *Angew. Chem., Int. Ed.*, 2001, **40**, 1372–1409.
25 N. Martín, L. Sánchez, M. Á. Herranz, B. Illescas and D. M. Guldi, *Acc. Chem. Res.*, 2007, **40**, 1015–1024.
26 J. Garín, J. Orduna, S. Uriel, A. J. Moore, M. R. Bryce, S. Wegener, D. S. Yufit and J. A. K. Howard, *Synthesis*, 1994, 489–493.
27 G. Cooke, F. M. Duclairoir, V. M. Rotello and J. F. Stoddart, *Tetrahedron Lett.*, 2000, **41**, 8163–8166.
28 M. Á. Herranz, L. Yu, N. Martín and L. Echegoyen, *J. Org. Chem.*, 2003, **68**, 8379–8385.
29 P. Daum and R. W. Murray, *J. Electroanal. Chem. Interfacial Electrochem.*, 1979, 103, 289–294.
30 H. L. Lord, W. Zhan and J. Pawliszyn, *Fundamentals and applications of needle trap devices*, John Wiley & Sons, Inc., New York, NY, 2012, vol. 2.
31 M. Lyons, in *Electroanalytical Chemistry*, ed. A. J. Bard and I. Rubisntein, Marcel Dekker, Inc, New York, NY, 2014, p. 110.
32 O. Alévêque, F. Seladji, C. Gautier, M. Dias, T. Breton and E. Levillain, *ChemPhysChem*, 2009, **10**, 2401–2404.
33 Y. Yokota, A. Miyazaki, K. I. Fukui, T. Enoki, K. Tamada and M. Hara, *J. Phys. Chem. B*, 2006, **110**, 20401–20408.
34 P.-Y. Blanchard, O. Alévêque, S. Boisard, C. Gautier, A. El-Ghayoury, F. Le Derf, T. Breton and E. Levillain, *Phys. Chem. Chem. Phys.*, 2011, **13**, 2118–2120.
35 E. Barsoukov and J. R. Macdonald, *Impedance Spectroscopy: Theory, Experiment, and Applications*, 2005.
36 S. Campuzano, M. Pedrero, C. Montemayor, E. Fatás and J. M. Pingarrón, *J. Electroanal. Chem.*, 2006, **586**, 112–121.
37 E. Boubour and R. B. Lennox, *J. Phys. Chem. B*, 2000, **104**, 9004–9010.
38 J. N. Murray, *Prog. Org. Coat.*, 1997, **31**, 375–391.
39 L. V. S. Philippe, G. W. Walter and S. B. Lyon, *J. Electrochem. Soc.*, 2003, **150**, B111–B119.
40 J. R. Macdonald and W. B. Johnson, *Fundamentals of Impedance Spectroscopy*, 2005.
41 T. M. Nahir and E. F. Bowden, *Langmuir*, 2002, **18**, 5283–5286.
42 E. Katz, O. Lioubashevsky and I. Willner, *J. Am. Chem. Soc.*, 2004, **126**, 15520–15532.
43 Y. Guo, J. Zhao, X. Yin, X. Gao and Y. Tian, *J. Phys. Chem. C*, 2008, **112**, 6013–6021.
44 R. E. Ruther, Q. Cui and R. J. Hamers, *J. Am. Chem. Soc.*, 2013, **135**, 5751–5761.
45 M. Drüschler, N. Borisenko, J. Wallauer, C. Winter, B. Huber, F. Endres and B. Roling, *Phys. Chem. Chem. Phys.*, 2012, **14**, 5090.
46 Z. Kerner and T. Pajkossy, *Electrochim. Acta*, 2000, **46**, 207–211.
47 E. Boubour and R. B. Lennox, *Langmuir*, 2000, **16**, 4222–4228.
48 P. R. Bueno, G. Mizzon and J. J. Davis, *J. Phys. Chem. B*, 2012, **116**, 8822–8829.
49 M. S. Góes, H. Rahman, J. Ryall, J. J. Davis and P. R. Bueno, *Langmuir*, 2012, **28**, 9689–9699.
50 P. R. Bueno, F. Fabregat-Santiago and J. J. Davis, *Anal. Chem.*, 2013, **85**, 411–417.
51 G. Yzambart, B. Fabre, F. Camerel, T. Roisnel and D. Lorcy, *J. Phys. Chem. C*, 2012, **116**, 12093–12102.
52 N. Bellec, A. Faucheux, F. Hauquier, D. Lorcy and B. Fabre, *Int. J. Nanotechnol.*, 2008, **5**, 741–756.

 This journal is © The Royal Society of Chemistry 2017

53 V. F. Lvovich, *Impedance spectroscopy application to electrochemical and dielectric phenomena*, Wiley, 2012.
54 M.-J. Lee, C. B. Lee, D. Lee, S. R. Lee, M. Chang, J. H. Hur, Y.-B. Kim, C.-J. Kim, D. H. Seo, S. Seo, U.-I. Chung, I.-K. Yoo and K. Kim, *Nat. Mater.*, 2011, **10**, 625–630.
55 R. Waser, R. Dittmann, C. Staikov and K. Szot, *Adv. Mater.*, 2009, **21**, 2632–2663.
56 T. Chattopadhyay, J. N. Roy and A. K. Chakraborty, *Opt. Commun.*, 2009, **282**, 1287–1293.

Open Access Article. Published on 17 January 2017. Downloaded on 17/01/2017 14:25:40.
This article is licensed under a Creative Commons Attribution 3.0 Unported Licence.

Electronic Supplementary Material (ESI) for RSC Advances.
This journal is © The Royal Society of Chemistry 2016

Supporting Information

A four-state capacitance molecular switch based on a redox active tetrathiafulvalene self-assembled monolayer

E. Marchante[a], M.S. Maglione[a], N. Crivillers[a], C. Rovira[a] and M. Mas-Torrent[a,*]

Table of contents

Synthesis of TTF molecule (**1**)

TTF **1** was synthesized according to the following scheme:

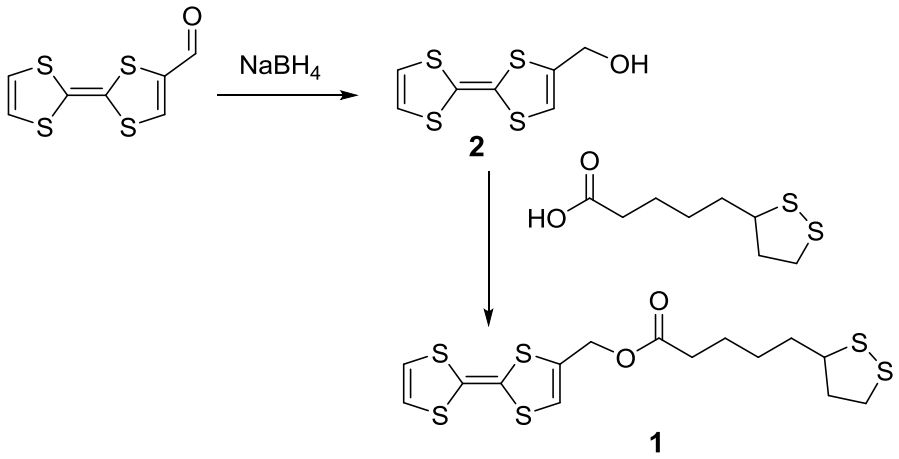

Synthesis of [2,2'-bi(1,3-dithiolylidene)]-4-ylmethanol[1] (2)

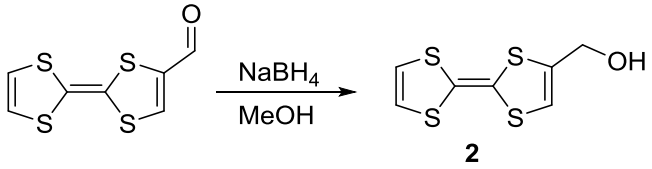

To a solution of 2-formyltetrathiafulvalene (500 mg, 2.15 mmol) in MeOH (20 mL), it was added $NaBH_4$ (89 mg, 2.36 mmol). The solution was stirred during 30 minutes. CH_2Cl_2 was then added and the mixture was washed with brine and water. The organic phase was isolated, dried over $MgSO_4$ and concentrated under reduced pressure. The yellow solid thus obtained was purified by column chromatography (silica gel) using CH_2Cl_2. Compound **2** was obtained in a 96% yield.

IR: (v/cm^{-1}): 3290; 3057; 2925; 2857; 1542; 1456; 1114; 109; 1016; 793; 767; 648; 628.

^{1}H NMR (250 MHz CD_2Cl_2): δ= 6.35 (s 2H); 6.24 (s, 1H); 4.37 (s, 2H) 1.96 (s, 1H).

^{13}C NMR (400 MHz CD_2Cl_2): δ=137.43; 119.54; 119.47; 115.50; 111.50; 109.86; 60.96.

LDI-TOF (m/z): calculated: 234.3; experimental: 233.9 ([M^+]).

Synthesis of [2,2'-bi(1,3-dithiolylidene)]-4-ylmethyl 5-(1,2-dithiolan-3-yl)pentanoate[2] (1)

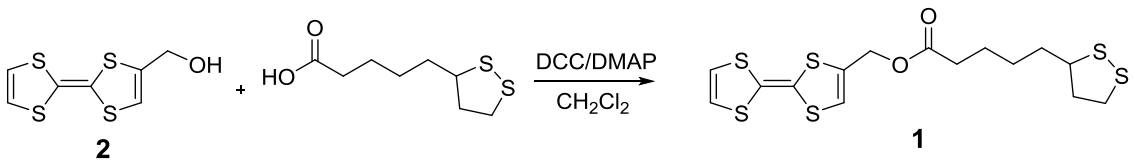

[1] J. Gran, J. Orduna, S.Uriel A.J.Moore, M.R. Bryce, S.Wegener, D.S.Yufit, J.A.K..Howard *Synthesis*, **1994**, 489-493

[2]G.Cooke, F. Duclairoir, V. Rotello, M, J.Stoddart *Tetrahedron Letters* **2000**, 41, 8163-8166. M. A. Herranz, L. Yu, N. Martín, L. Echegoyen *J. Org. Chem.* **2003**, 68, 8379-8385

To 40 mL of CH_2Cl_2 previously filtered through basic alumina, compound **2** (290 mg, 1.23 mmol) and thioctic acid (305 mg, 1.48 mmol) were added. The mixture was stirred under N_2 at 0ºC during 15 minutes. A solution of DCC (379 mg, 1.84 mmol) and DMAP (45 mg, 0.37 mmol) in 10 mL of CH_2Cl_2 was added and the mixture was kept stirring for 15 minutes at 0º C. The solution was then allowed to reach room temperature and was left under stirring for another 24 h. The reaction mixture was then washed with water, the organic layer was dried under $MgSO_4$ and the solvent was evaporated under reduced pressure. The crude of the reaction was purified by silica column chromatography using CH_2Cl_2 as eluent and compound **1** was obtained with a 90% yield.

IR: (v/cm^{-1}): 3062; 2925; 2824; 1728; 1578; 1518; 1456; 1389; 1151; 1125; 661; 570.

^{1}H NMR (400 MHz, CD_2Cl_2):δ= 6.36(s, 1H)-6.35 (s, 2H); 4.81 (s, 2H) 3.60-3.54 (m, 1H); 3.20-3.07 (m, 2H); 2.49-2.41 (m, 1H); 2.36 (t, J=7.3 Hz, 2H); 1.94-1.86 (m, 1H) 1.74-1.61 (m, 4H); 1.51-1.41 (m 2H).

^{13}C NMR (500 MHz CD_2Cl_2): δ=172.81; 131.41; 119.19; 119.16; 119.08, 111.55; 109.05; 60.58; 56.38; 40.23; 38.55; 34.56; 33.73; 28.65; 24.60.

LDI-TOF (m/z): calculated: 422.6; experimental: 421.9 ([M$^+$]).

Experimental methodologies

Materials and reagents. HPLC solvents, dichloromethane, acetone, absolute ethanol, isopropanol, tetrahydrofuran and acetonitrile were supplied by Teknokroma. Lithium perchlorate ($LiClO_4$) was purchased from Aldrich and used as received. Gold (111) substrates consisting of 300 nm Au on mica were purchased from Georg Albert PVD-Beschichtungen.

2-formyltetrathiafulvalene was purchased from TCI Chemicals, while $NaBH_4$ and thioctic acid were bought from Sigma-Aldrich. All the reagents were used without further purification.

Experimental procedures and apparatus

Self-assembled monolayers preparation. The substrates were first rinsed with dichloromethane, acetone and ethanol and dried under nitrogen stream. Then, these substrates were cleaned in a UV ozone chamber for 20 minutes and afterwards immediately immersed in ethanol for at least 20 minutes, rinsed with ethanol and isopropanol and dried under N_2 stream. Subsequently, the substrates were immediately immersed in 1mM solution of **1** in tetrahydrofuran for 72h. SAM formation was carried out under light exclusion and under nitrogen atmosphere.

XPS Measurements. X-ray photoelectron spectroscopy measurements were performed with a Phoibos 150 analyzer (SPECS GmbH, Berlin, Germany) in ultra-high vacuum conditions (base pressure 5x10^{-10} mbar) with a monochromatic aluminium Kalpha X-ray source (1486.74eV). The energy resolution measured by the FWHM of the Ag 3d5/2 peak for a sputtered silver foil was 0.6 eV. The spot size was 3.5 mm by 0.5 mm.

ToF-SIMS Measurements. Time of flight secondary ions mass spectrometry measurements were performed with a TOF-SIMS5 using the following specific conditions of analysis: primary gun energy of 25 KV; extractor energy of 10 KV; an emission current 1.00 µA; employing Bi3+ with an intensity of the primary ions of 0.26 pA. The experiments were performed under vacuum at 2.3 E-9 mbar. The spot size was 250 x 250 µm with a resolution of 128 x 128 pixels, collecting above of 1 E12 of ionic intensity per spectrum.

Cyclic Voltammetry measurements. Cyclic voltammetry experiments were performed using a Novocontrol modular equipment system which consists on an Alpha-AN impedance analyzer with a POT/GAL 30V/2A electrochemical interface. A conventional three electrode set-up was employed using the modified gold substrate as the working electrode, a platinum wire as counter electrode and a silver wire as quasi-reference electrode. We have used a homemade electrochemical cell with a control active area of the functionalized substrate (i.e. working electrode) of 0.5 cm^2. A degasificated solution of $LiClO_4$ 0.1 M in acetonitrile was used as electrolyte (after bubbling N_2 for 20 min).

Electrochemical Impedance Spectroscopy (EIS) measurements: The impedance measurements were obtained at four different DC potentials, and were superimposed on a sinusoidal potential modulation of ±5 mV (V_{rms}). The resulting current was recorded over a frequency domain of 200 KHz to 500 mHz. Ninety points, equally spaced on a logarithmic scale, were acquired per decade increment in frequency. All experiments were performed at room temperature and under environmental conditions.

Switching Measurements. The AC impedance switching process was recorded at 1Hz. A low AC voltage of 5 mV was superimposed at four different applied DC bias (10, 250, 450 and 620 mV). These cycling experiments were performed by pre-biasing the sample at the corresponding DC voltage for each state during 3 seconds.

Supporting information figures:

Table S1. Summary of the binding energies observed in the high-resolution XPS characterization of the TTF SAM

Binding energy (eV)	Atom	Type of bond
532.2	O1s	C-O
333.3	O1s	C=O
284.8	C1s	C-C
285.7	C1s	C=C
288.9	C1s	O-C=O
161.9	$S2p_{3/2}$	S-Au
163.1	$S2p_{1/2}$	S-Au
163.6	$S2p_{3/2}$	C-S-C
164.7	$S2p_{1/2}$	C-S-C

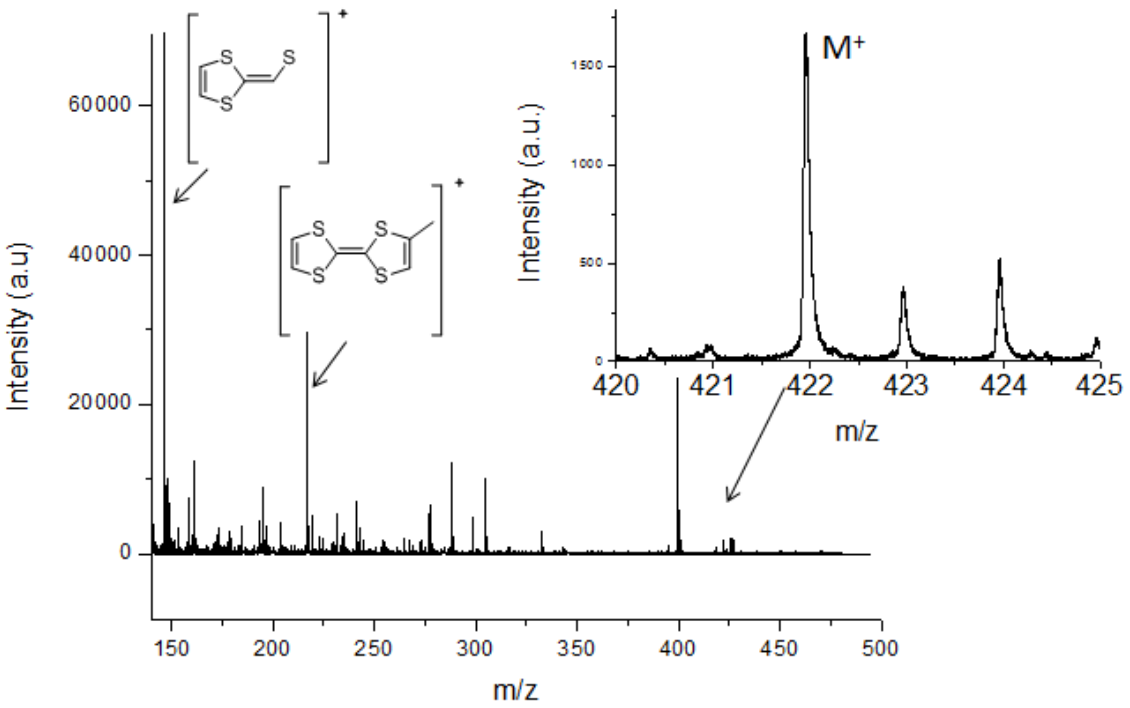

Figure S1. ToF-SIMS spectrum for TTF SAM.

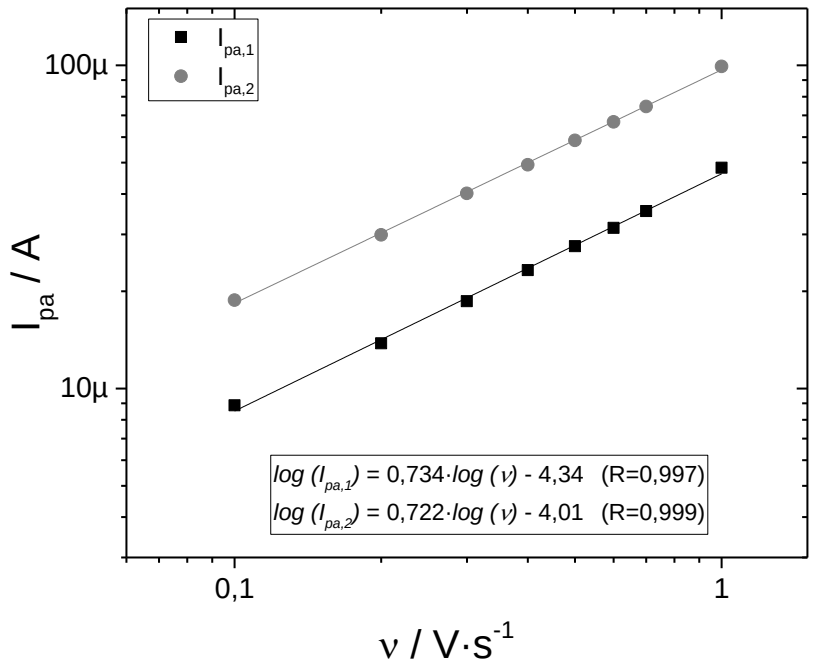

Figure S2. Linear relationship of the current peak ($I_{p,a}$) *vs* the scan rate (ν) for the two redox processes observed in the TTF SAM on gold.

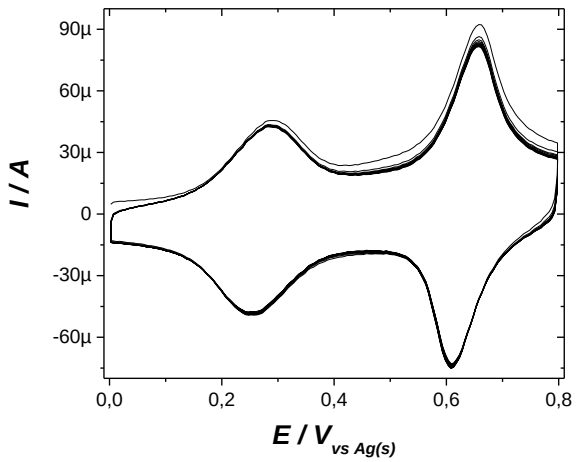

Figure S3. CV of the TTF SAM in $LiClO_4$ 0.1M in acetonitrile, at 1V/s, during 10 cycles.

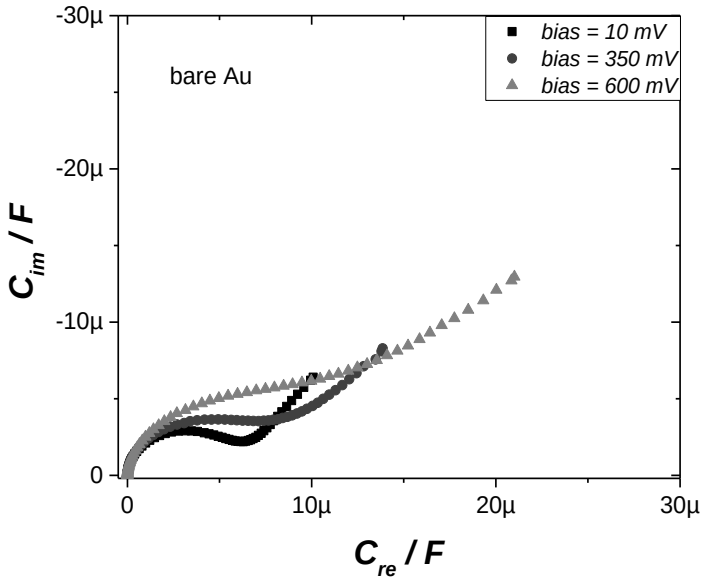

Figure S4. Capacitance Cole-Cole plot of the unmodified Au substrate in $LiClO_4$ 0.1 M in acetonitrile at three DC voltages (10 mV, 350 mV and 600 mV).

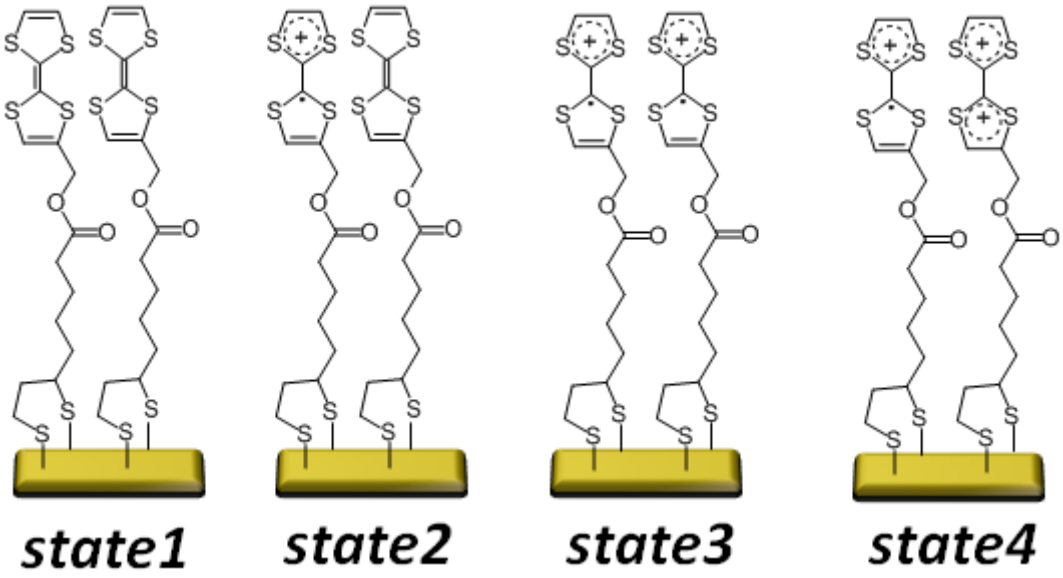

Figure S5. Scheme of the TTF-SAM states at the four different DC bias applied: 10 mV (state 1), 250 mV (state 2), 450 mV (state 3), and 620 mV (state 4).

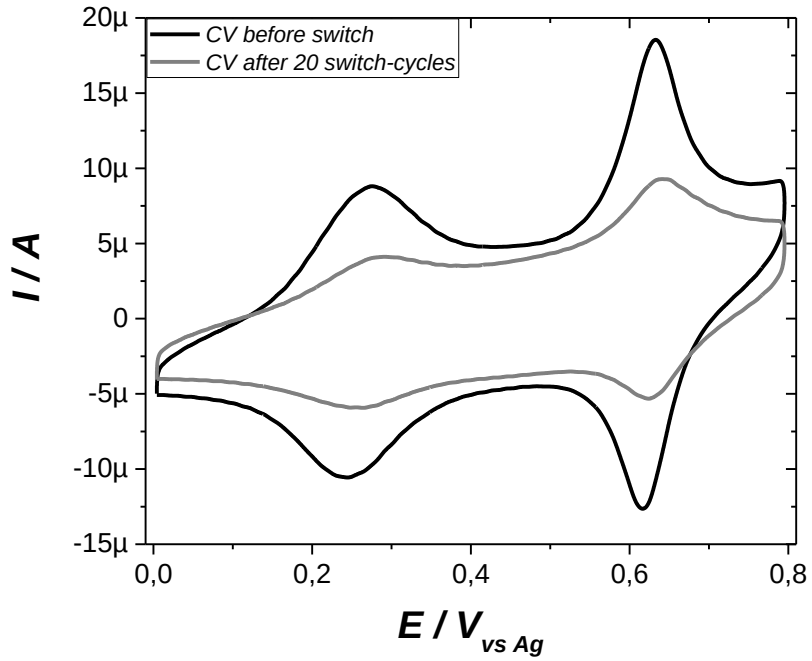

Figure S6. CV of the TTF SAM in $LiClO_4$ 0.1M in acetonitrile before and after the 20 switching cycles performed by EIS.

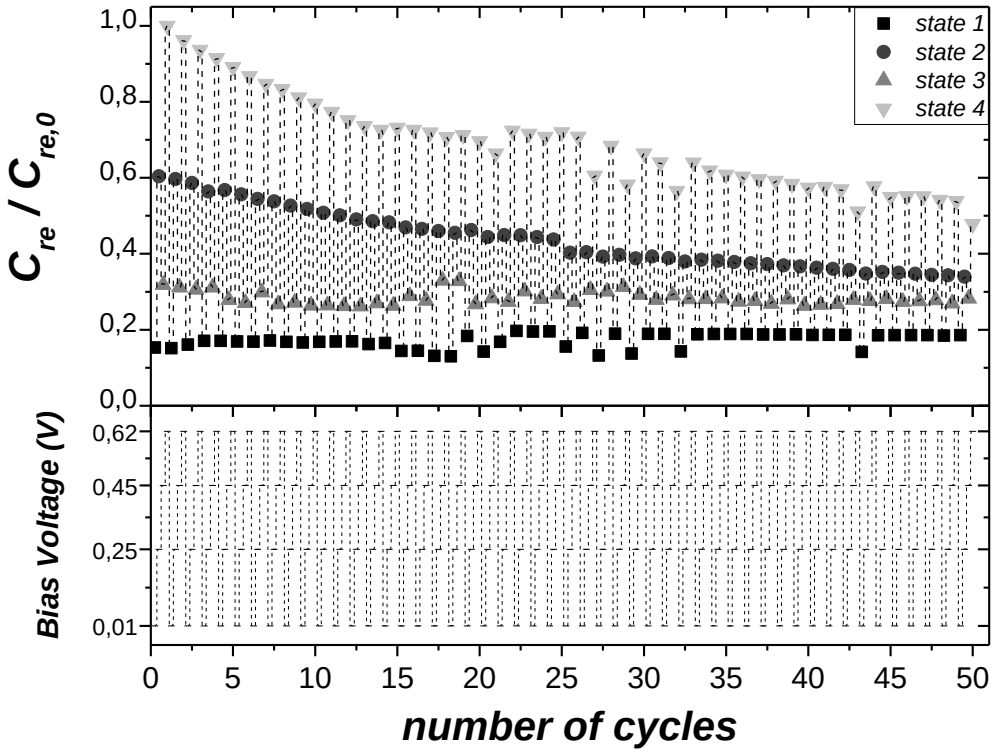

Figure S7. Relative capacitance values of a TTF-SAM during 50 switching cycles.